

CHAPTER 3

Results and discussion

3.1 QSAR analysis

3.1.1 QSAR model generation

There are 2 steps for selection of appropriate descriptors to generate a MLR model. First, 376 molecular descriptors that were not significantly correlated with the P-gp modulatory activity ($r < 0.1$) were excluded from total 1,252 descriptors. Second, the remaining 876 descriptors were determined the pairwise correlation coefficient resulting in the removal of 570 descriptors. The remaining 306 descriptors were chosen using stepwise linear regression variable selection method. A stepwise multiple linear regression analysis was operated utilising the remaining descriptors after selection as inputting variables. The 23 flavonoids in the training set were utilised to create a statistical model equation between the P-gp modulatory (pFAR) values and their physicochemical descriptors. In accordance with the criteria, six physicochemical descriptors were involved in equation, which include RDF_PiChg_86, RDF_SigChg_76, 3DACorr_TotChg_9, RDF_LpEN_54, 3DACorr_PiChg_9, and RDF_SigChg_57. The intercorrelations between the six descriptors are shown in Table 3.1. The pFAR was represented by the ensuing equation:

$$\text{pFAR} = \Sigma(C_i D_i) + D_c$$

where D_c is a constant, D_i is a descriptor and C is its corresponding regression coefficient in multiple linear regression models. The corresponding regression coefficients are shown in the following model.

The selected model, $\text{pFAR} = -0.61(\text{RDF_PiChg_86}) + 0.46(\text{RDF_SigChg_76}) - 0.28(\text{3DACorr_TotChg_9}) + 0.21(\text{RDF_LpEN_54}) - 0.28(\text{3DACorr_PiChg_9}) - 0.20(\text{RDF_SigChg_57}) - 0.42$, was found to have values in the required range and the regression parameters and quality correlation of the significant regression equation are $N=23$, $R=0.963$, $R^2=0.927$, $R^2_{adj}=0.900$, $SEE=0.197$, $F=33.849$, $p<0.001$ and internal

validation (LOO method) $q^2=0.927$ (N is the number of compound in the training set, R is the correlation coefficient, R^2 is the coefficient of determination, R^2_{adj} is the adjusted coefficient of determination, SEE is the standard error of estimate, F is the Fisher test and q^2 is the cross-validated r^2).

Table 3.1 Correlation matrix indicating intercorrelation among descriptors used in MLR QSAR model

pFAR	RDF_Pi Chg_86	RDF_SigChg_76	3DACorr_TotChg_9	RDF_LpEN_54	3DACorr_PiChg_9	RDF_SigChg_57
RDF_Pi Chg_86	1					
RDF_SigChg_76	0.288	1				
3DACorr_TotChg_9	0.572	0.377	1			
RDF_Lp EN_54	0.529	-0.035	0.448	1		
3DACorr_PiChg_9	-0.745	-0.315	-0.299	-0.290	1	
RDF_SigChg_57	0.444	0.629	0.287	-0.033	-0.477	1

RDF_PiChg_86 is the radial distribution functions weighted by π charges, where r is in the range of 8.5 to 8.6 Å.

RDF_SigChg_76 is the radial distribution functions weighted by σ atom charges, where r is in the range of 7.5 to 7.6 Å.

3DACorr_TotChg_9 is the 3D autocorrelation weighted by total atom charges (sum of σ , π charges), where d is in the range of 9–10 Å

RDF_LpEN_54 is the radial distribution functions weighted by lone pair electronegativities, where r is in the range of 5.3 to 5.4 Å.

3DACorr_PiChg_9 is the 3D autocorrelation weighted by π atom charges, where d is in the range of 9–10 Å

RDF_SigChg_57 is the radial distribution function weighted by σ charge, where r is in the range of 5.6 to 5.7 Å.

In addition, the prediction results of pFAR are listed in Table 3.2 and the plot of observed (experimental) versus calculated (predicted) pFAR values is shown in Figure 3.1 that illustrates correlation between observed and calculated values utilising the model and corresponding regression equation. The coefficients of slope and intercept are close to the ideal condition (slope = 1 and intercept = 0). This information could be respected as expedient alternative to testify validity of a QSAR model (Shayanfar et al., 2016).

ลิขสิทธิ์มหาวิทยาลัยเชียงใหม่
Copyright © by Chiang Mai University
All rights reserved

Table 3.2 The observed and calculated pFAR values using the developed QSAR equation with associated residuals

Compound no.	Observed pFAR	Predicted pFAR	Residual
1	-1.26	-1.20	-0.06
2	-1.67	-1.54	-0.13
3	-0.49	-0.63	0.14
4	-0.48	-0.34	-0.13
5	-0.45	-0.52	0.07
6	-1.46	-1.39	-0.07
7	-0.46	-0.47	0.01
8	-0.45	-0.42	-0.03
9	-0.36	-0.16	-0.20
10	-1.16	-1.38	0.22
11	-0.18	-0.27	0.09
12	-0.69	-0.60	-0.09
13	0.22	0.12	0.10
14	0.15	0.03	0.12
15	0.15	-0.09	0.25
16	0.10	0.32	-0.22
17	0.30	0.21	0.10
18	0.22	0.25	-0.03
19	0.10	0.30	-0.20
20	-0.38	-0.34	-0.04
21	-1.56	-1.34	-0.22
22	0.01	-0.44	0.45
23	0.24	0.36	-0.13

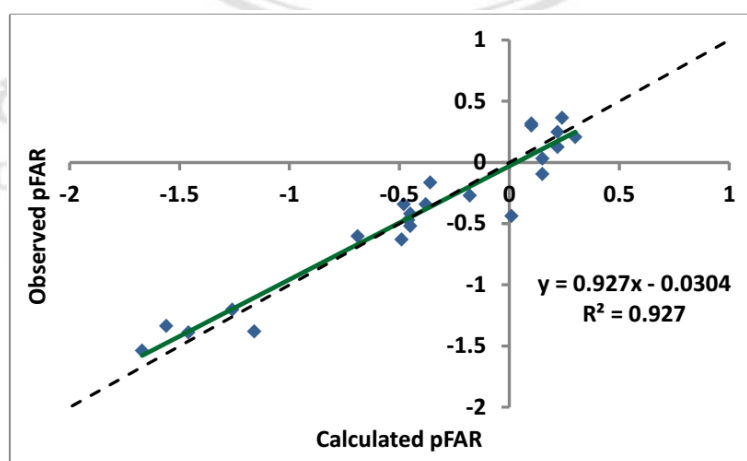


Figure 3.1 A plot of observed (experimental) versus calculated (predicted) pFAR values of the training set

3.1.2 P-gp modulation prediction using the external test set of flavonoids for validation of the calculated QSAR model

The model with 6 selected molecular descriptors, which provided a good prediction operation on the external test set (Table 3.3), possessed high prediction accuracy that can predict the P-gp modulatory activity of 7 (from all 11) flavonoid compounds correctly including naringenin, quercetin, morin, EGCG, ECG, biochenin A and hesperidin. It could be seen that the most of the predicted flavonoid compounds showed the range of low to high predicted P-gp inhibitory activities.

From the test set, silymarin, 5-Hydroxy-3,6,7,8,3',4'-hexamethoxyflavone (5HHMF) and nobiletin exhibited experimental active P-gp inhibitory activities but they were wrongly predicted to be P-gp inducers with the calculated pFARs were 0.42, 0.44 and 1.58 respectively. Demethylnobiletin exhibited an experimental active P-gp inhibitory activity but its predicted activity was slightly discrepant estimated to be a strong inhibitor (calculated pFAR = -1.13). These flavonoids are a polymethoxyflavone (PMF) that contains many methyl functional groups whereas the most molecules in the training set are not PMF. For this reason, it may result in missing of P-gp modulatory activity prediction for these compounds in the test set.

Some descriptors including RDF_LpEN_54 of silymarin, RDF_PiChg_86 and RDF_SigChg_57 of nobiletin and RDF_SigChg_57 of demethylnobiletin used in the MLR QSAR model were outlier values that may cause the discrepant prediction of P-gp modulatory activity.

ลิขสิทธิ์มหาวิทยาลัยเชียงใหม่
Copyright © by Chiang Mai University
All rights reserved

Table 3.3 Comparison between the calculated P-gp modulatory activity values (pFAR) and observed values of 11 flavonoids which exhibited a significant experimental P-gp inhibitory activity expressed by Inhibitory efficiency

Compound	Inhibitory efficiency (observed activity) ^a	Classification (by observed activity)	Calculated pFAR (Predicted activity)	Classification (by predicted activity)
Naringenin	56.93	Active inhibitor	-0.39	Active inhibitor ^b
Quercetin	72.73	Active inhibitor	-0.04	Active inhibitor ^b
Morin	56.63	Active inhibitor	-0.07	Active inhibitor ^d
Silymarin	60	Active inhibitor	0.42	Inducer ^d
Epigallocatechingallate (EGCG)	168.18	Strong inhibitor	-1.03	Strong inhibitor ^c
Epicatechingallate (ECG)	95.45	Active inhibitor	-0.61	Active inhibitor ^c
Biochanin A	198.04	Strong inhibitor	-1.30	Strong inhibitor ^b
Hesperidin	164.41	Strong inhibitor	-1.32	Strong inhibitor ^e
Demethylnobiletin	87.43	Active inhibitor	-1.13	Strong inhibitor ^e
5HHMF	65.47	Active inhibitor	0.44	Inducer ^e
Nobiletin	45.71	Active inhibitor	1.58	Inducer ^e
Positive control (verapamil)	100	Strong inhibitor	-	-

^a Inhibitory efficiency calculated as percentage compared to a positive control; verapamil, ^b From Chung et al. (Chung et al., 2005), ^c From Kitagawa et al. (Kitagawa et al., 2004), ^d From Zhang and Morris (Zhang & Morris, 2003), and ^e From El-Readi et al. (El-Readi et al., 2010)

The application of medicinal plants in a variety of therapies around the world uplifts the question regarding their safety and evidence-based efficacy. Unprecedented and significant herb–drug interactions may emerge and put individuals at hazard, especially those people who utilise multiple medicines. The data regarding herb–drug interactions is needy, derived mostly from *in vitro*, *in vivo* and including clinical studies that cannot be directly operated in every infirmary. By reason of that, it is essential to conduct *in silico* or computational studies as a preliminary screening with enough potency before henceforth study in humans.

Many medicinal plants have been already known to induce or inhibit transporters like P-gp which are recognised as vicarious drug transporter. Therefore, a summary of cognition on the modulation of P-gp by ordinarily utilised herbs can allow vigorous fundamentals for optimising P-gp substrate drug-based remedy. In this case, we study

bioflavonoids as offenders of P-gp-mediated pharmacokinetic herb-drug interactions. The major focus is on the potentiality of phytochemicals which are plant-derived flavonoids to modulate the transport function of P-gp. Normally, the first step in determination of herb–drug interaction is well chemical definition of herbal products. The flavonoids utilised in our experiments were from previously published literatures and mainly clarified as responsible for P-gp modulatory effects.

This work used vast (1252) molecular descriptors on the basis of both two and three-dimensional molecular structures. As shown in the model, the analysis in term of radial distribution functions (RDF codes) are predominating factors that influence to prediction of the activity of P-gp modulators. Among the selected six descriptors, four RDF codes based on pi (π) and sigma (σ) atom charges, and also lone pair electronegativities were selected (RDF_PiChg_86, RDF_SigChg_76, RDF_SigChg_57, RDF_LpEN_54), respectively which point out that the representation of molecular structures of the P-gp modulators is considerably attribute to the atom RDF properties of 3D structures of flavonoid molecules. RDF codes also have high correlations with the induced/ inhibitory activities and they are such powerful descriptors for representation of the characteristics of a molecule thoroughly. In accordance with this study, Boccard et al. (Boccard et al., 2009) analysed a set of 83 flavonoids which exhibited the binding affinity to nucleotide binding site 2 (NBD2) represented by K_d values (dissociation constants) that were converted to $-\log K_d$. Then the three-dimension linear solvation energy model was built using partial least-squares (PLS) analysis as a statistical method for generation of a 3D-QSAR equation from Volsurf descriptors. The internal predictivity was shown by $r^2 = 0.76$ and $q^2 = 0.71$ and lower than predictivity of our model. This 3D model revealed the robust influence of 3D descriptors related to 3D shape of flavonoid molecule.

The antioxidant properties of bioflavonoids are dependent on their expansive conjugated π -electron systems grant ready donation of electrons or hydrogen atoms from the hydroxyl moieties to free radicals (McPhail, Hartley, Gardner, & Duthie, 2003) and RDF_PiChg_86 has the highest correlation coefficients with the P-gp modulatory activity of flavonoids. Moreover, the selection of 3DACorr_PiChg_9 means that the 3D autocorrelation π charge may likewise affect the P-gp modulatory activity of a compound. That is to say with the increase of vectorial molecular descriptors derived

from 3D structure of a molecule weighted by π charges (RDF_PiChg_86 and 3DACorr_PiChg_9) elevated P-gp inhibitory activity.

Furthermore, RDF_SigChg_76 and RDF_SigChg_57 (weighted by σ atom charges), including a 3D autocorrelation descriptor; 3DACorr_TotChg_9 weighted by total atom charge (which are the summation of σ and π charges) and RDF_LpEN_54 which is weighted by lone pair electronegativities were likewise chosen as independent variables in the model. RDF_SigChg_76 and RDF_LpEN_54 with positive coefficients, which means the molecular properties relied on σ atom charges in the range of 7.5 to 7.6 Å of flavonoid molecule and lone pair electronegativities involved a contribution of the P-gp induced activity of flavonoids, on the other hand, RDF_SigChg_57, and 3DACorr_TotChg_9 with negative coefficients contributed to the P-gp inhibitory activity. It indicates that with the going up of molecular physicochemical properties weighted by total atom charges (which are the summation of σ and π charges), the inhibitory activity of P-gp will increase.

Sheu et al. (Sheu et al., 2010) constructed the empirical QSAR models for prediction of P-gp modulation effects using 4 major subclasses of 23 flavonoids including flavones, flavonols, flavanones, and isoflavones as a training set. A stepwise regression analysis was used to generate the model with P-gp induction or inhibition as a dependent variable and independent variables including the presence of structural units and skeletons, physicochemical properties (molecular weight, solubility parameter, and octanol-water partition coefficient). The most three optimal constructed QSAR models showed adjusted $R^2 = 0.6809$, 0.5902 , and 0.4798 respectively but no standard error of estimation (*SEE*) was shown, while our MLR QSAR model possesses higher value. Considering another study, Wang et al. (Wang et al., 2005) constructed QSAR model using Bayesian-regularised neural network (BRNN) technique as a regression method from the dataset comprised of fifty-seven flavonoids with binding ability to NBD2 of P-gp expressed by K_d values and utilising Molconn-Z programme for calculation of molecular descriptors of these structures. Concerning when using the optimum QSAR model obtained by this technique for calculation of predicted K_d of flavonoids in the training set provided $R^2 = 0.756$ $SEE = 0.120$ of observed versus predicted values while our QSAR model provided $R^2 = 0.927$ with $SEE = 0.204$ which

are alike and that indicated MLR method utilised in our study provided trustful QSAR model for prediction of P-gp modulation.

The P-gp modulatory activity of 23 flavonoids was studied based on QSAR modelling by a stepwise multiple linear regression analysis. The ADRIANA.Code programme has a capacity for a unique combination of methods for the calculation of molecular structure descriptors and molecular properties of the molecules of flavonoids based on a sound geometric and physicochemical basis. Furthermore, it contains a hierarchy of incremental levels of sophistication in superseding chemical compounds from constitution to three-dimensional structure, to the surface of a molecule. For the training and test sets, 1252 molecular descriptors were calculated in short computation time from the SMILES notation available for each compound (Kovalishyn et al., 2011; Li et al., 2014; Yan et al., 2008). The computational results of the model generation suggested that among the selected 6 descriptors, 4 descriptors were the RDF codes indicating the RDF codes had significant correlation with P-gp modulatory activity. They are forceful descriptors for representation of the three-dimensional structure and characteristics of the flavonoid molecule thoroughly. Additionally, it was also found that the molecular properties relied on atom charges (both σ and π charges) and including lone pair electronegativities were greatly correlated with the P-gp modulatory activity of flavonoids. This developed QSAR model has been discovered capable for predicting some molecular properties, and the graceful model gained in this study can be then utilised to estimate the P-gp modulatory activity for other flavonoids.

Quality and safety evaluation of herb are downright important for raising popularisation of food as medicine throughout the world. The present study determined the conceivable herb-drug interactions potential of flavonoid-containing medicinal plants with their bioactive compounds used as dietary supplements in a modern system of medicine. Result indicated that some flavonoids having high inhibitory activity values than positive inhibitor such as verapamil against different P-gp. However, it can be concluded that possibilities of herb-drug interaction of flavonoids and prescription drugs are very risky if these compounds are administered concomitantly and the botanical products may produce any toxic effects due to inhibition of P-gp action consequently increasing bioavailability of phytochemicals in a body. Some other significant factors of metabolism like the competition among co-administered herbs or

drugs, nonspecific interactions with proteins and enzyme induction by reason of chronic intake etc. are a necessity to be determined henceforward.

It is interesting to notice that many natural flavonoids can modulate P-gp activity. The developed ligand-based (QSAR) and structure-based pharmacophore models obtained from our study are useful to screen a potential inhibitory activity of flavonoids that can be applied in anti-cancer drug development and herb-drug interaction analysis via the mechanism of P-gp inhibition.

3.2 Molecular docking

3.2.1 Docking of P-gp inhibiting compounds against NBD1

Docking of the 25 flavonoids against NBD1 was conducted. The optimal pose of each compound with the lowest estimated free energy of binding ranging from -7.96 to -5.77 kcal/mol were then used for further linear regression analysis. Notably, the more negative the estimated free energy of binding value was, the higher the predicted value was 8 flavonoids (amorphigenin, epigallocatechin, rotenone, formononetin, chrysin, epigallocatechingallate, biochanin A, and hesperidin) exhibited *in vitro* strong P-gp inhibitory activity showed low estimated free energy of binding values ranging from -7.96 to -7.10 kcal/mol. Other 17 flavonoids exhibited *in vitro* active (weak) P-gp inhibitory activity had relatively higher estimated free energy of binding values ranging from -7.08 to -5.77 kcal/mol. 3 known P-gp inhibitors (verapamil, nifedipine, and atorvastatin) used as positive controls, 1 non P-gp inhibitor (captopril), and 1 P-gp substrate (ATP) also were conducted docking. It was shown that verapamil which is a strong inhibitor of P-gp was of low estimated free energy of binding (-6.66 kcal/mol); and the moderate P-gp inhibitor (nifedipine) and the weak P-gp inhibitor (atorvastatin) were of relatively higher energies (-6.15 and -5.68 kcal/mol respectively). The inhibition of flavonoids on the metabolism of ATP depended on whether their free energies of binding were much lower than that of ATP or not. The estimated free energy of binding of natural substrate of P-gp (ATP) was -5.62 kcal/mol which was considered to be the threshold of positive binding and the estimated free energy of binding of all the test compounds was much lower than -5.62 kcal/mol, showing that they all can bind to the catalytic site of NBD1 (Table 3.4). Regarding the non P-gp inhibitor; captopril, it was of the lowest binding affinity to NBD1 of P-gp with the highest docking score -4.79

kcal/mol. Table 3.5 illustrates the complete profile of parameters of free energy of binding as final intermolecular energy, total estimated energy of vdW+Hbond+desolv, electrostatic energy, final total internal energy, torsional free energy, and unbound system's energy were evaluated to estimate the favourable binding of all flavonoids and controls for their interaction with NBD1. A calculation of estimated free energy of binding of each flavonoid from these parameters is shown under the table.

Table 3.4 The experimental P-gp inhibitory activity value expressed by percentage compared to a positive control (verapamil) and the docking score at NBD1 expressed by the estimated free energy of binding of each flavonoid

Flavonoid	Inhibitory efficiency unit	Percentage of activity compared to a positive control (verapamil)	Lowest Estimated Free Energy of Binding in Cluster (kcal/mol)	Estimated Inhibition Constant of the Selected Docking Pose, K_i (μ M)	Classification (by observed inhibitory activity)
	<i>pFAR</i> ^a				
Amorphigenin	-1.67	175.79	-7.96	1.47	Strong
Epigallocatechin	-1.56	164.21	-7.42	3.66	Strong
Rotenone	-1.46	153.68	-7.50	3.19	Strong
Formononetin	-1.26	132.63	-7.21	5.23	Strong
Chrysin	-1.16	122.11	-7.64	2.49	Strong
Floretin (Phloretin)	-0.69	72.63	-6.89	8.98	Active
Afomosisin	-0.49	51.58	-6.38	21.02	Active
6a,12a-Dehydroamorphigenin	-0.48	50.53	-6.67	12.89	Active
Catechin	-0.46	48.42	-6.51	16.93	Active
(+)-12-Hydroxyamorphigenin (Dabinol)	-0.45	47.37	-6.35	22.3	Active
Neohesperidin	-0.45	47.37	-6.71	12.0	Active
Sakuranetin	-0.38	40.00	-6.47	18.05	Active
Naringin	-0.36	37.89	-6.44	19.16	Active
Robinin	-0.18	18.95	-5.77	59.37	Active
Verapamil	-0.95	100	-6.66	13.03	Strong (positive control)
	<i>% of negative control on [³H]-daunomycin accumulation in MCF-7/ADR cells^b</i>				
Quercetin	201.8 \pm 16.4%	87.97	-6.89	8.87	Active
Naringenin	130.6 \pm 0.9%	56.93	-6.28	24.74	Active
Morin	129.9 \pm 2.6%	56.63	-6.53	16.23	Active
Verapamil	229.4 \pm 17.6%	100	-6.66	13.03	Strong (positive control)

Table 3.4 (continued)

Flavonoid	Inhibitory efficiency unit	Percentage of activity compared to a positive control (verapamil)	Lowest Estimated Free Energy of Binding in Cluster (kcal/mol)	Estimated Inhibition Constant of the Selected Docking Pose, K_i (μM)	Classification (by observed inhibitory activity)
<i>Accumulation ratio of rhodamine-123 in KB-C2 cells^c</i>					
Epigallocatechingallate (EGCG)	3.7	168.18	-7.73	2.17	Strong
Epicatechingallate (ECG)	2.1	95.45	-7.08	6.44	Active
Verapamil	2.2	100	-6.66	13.03	Strong (positive control)
<i>% of negative control on [³H]-daunomycin accumulation in MCF-7/ADR cells^d</i>					
Biochenin A	300	100	-7.10	6.25	Strong
Silymarin	180	60	-6.54	16.04	Active
Verapamil	300	100	-6.66	13.03	Strong (positive control)
<i>Inhibition efficiency (already converted from Fluorescence intensity of rhodamine123)^e</i>					
Hesperidin	164.41 ± 11.00	164.41 ± 11.00	-7.35	4.07	Strong
Demethylnobiletin	87.43 ± 20.45	87.43 ± 20.45	-6.79	10.52	Active
5-Hydroxy-3,6,7,8,3',4'-hexamethoxyflavone (5HHMF)	65.47 ± 13.16	65.47 ± 13.16	-6.53	16.3	Active
Nobiletin	45.71 ± 7.49	45.71 ± 7.49	-6.08	35.03	Active
Verapamil	100.00 ± 4.98	100.00 ± 4.98	-6.66	13.03	Strong (positive control)
<i>Positive control In vitro IC₅₀^f</i>					
Verapamil	10 μM	100	-6.66	5.98	Strong
Nifedipine	53 μM	18.87	-6.15	30.8	Moderate
Atorvastatin	96 μM	10.42	-5.68	57.37	Weak
<i>Negative control</i>					
Captopril	>1,000 μM	0	-4.79	308.52	Non active
<i>Substrate</i>					
Adenosine Triphosphate	-	-	-5.62	76.44	-

^a = (Gyéman et al., 2005; Martins et al., 2010), ^b = (Chung et al., 2005), ^c = (Kitagawa et al., 2004), ^d = (Zhang & Morris, 2003), ^e = (El-Readi et al., 2010), ^f = (Fenner et al., 2009)

Table 3.5 Composition of docking energy against NBD1 of each flavonoid

Flavonoid	Lowest Estimated Free Energy of Binding in Cluster (kcal/mol)	Final Intermolecular Energy (kcal/mol) (1)	vdW + Hbond + desolv Energy (kcal/mol) (a)	Electrostatic Energy (kcal/mol) (b)	Final Total Internal Energy (kcal/mol) (2)	Torsional Free Energy (kcal/mol) (3)	Unbound System's Energy (kcal/mol) (4)
Amorphigenin	-7.96	-9.45	-9.08	-0.36	-1.0	1.49	-1.0
Epigallocatechin	-7.42	-9.50	-9.27	-0.23	-2.31	2.09	-2.31
Rotenone	-7.50	-8.39	-8.42	0.03	-0.46	0.89	-0.46
Formononetin	-7.21	-8.1	-8.03	-0.07	-0.33	0.89	-0.33
Chrysin	-7.64	-8.54	-8.37	-0.17	-0.9	0.89	-0.9
Floretin (Phloretin)	-6.89	-9.27	-9.06	-0.21	-0.61	2.39	-0.61
Afromosin	-6.38	-7.57	-7.45	-0.13	-0.78	1.19	-0.78
6a,12a-Dehydroamorphigenin	-6.67	-8.16	-8.16	-0.01	-1.03	+1.49	-1.03
Catechin	-6.51	-8.30	-8.04	-0.26	-2.16	1.79	-2.16
(+)-12-Hydroxyamorphigenin (Dabnol)	-6.35	-8.14	-8.03	-0.1	-1.47	1.79	-1.47
Neohesperidin	-6.71	-11.19	-10.84	-0.35	-7.74	4.47	-7.74
Sakuranetin	-6.47	-7.66	-7.56	-0.1	-1.03	1.19	-1.03
Naringin	-6.44	-10.61	-10.18	-0.44	-5.75	4.18	-5.75
Robinin	-5.77	-11.43	-10.99	-0.45	-9.46	5.67	-9.46
Quercetin	-6.89	-8.68	-8.5	-0.18	-2.76	1.79	-2.76
Naringenin	-6.28	-7.48	-6.91	-0.57	-0.79	1.19	-0.79
Morin	-6.53	-8.32	-8.19	-0.13	-2.14	1.79	-2.14
Epigallocatechingallate (EGCG)	-7.73	-11.31	-11.15	-0.15	-4.92	3.58	-4.92
Epicatechingallate (ECG)	-7.08	-10.36	-10.15	-0.22	-3.69	3.28	-3.69
Biochenin A	-7.10	-8.29	-8.08	-0.21	-1.03	1.19	-1.03
Silymarin	-6.54	-9.23	-8.97	-0.25	-4.1	2.68	-4.1
Hesperidin	-7.35	-11.83	-11.55	-0.27	-6.34	4.47	-6.34
Demethylnobiletin	-6.79	-8.58	-8.64	0.06	-1.8	1.79	-1.8
5-Hydroxy-3,6,7,8,3',4'-hexamethoxyflavone (5HHMF)	-6.53	-8.62	-8.14	-0.48	-1.97	2.09	-1.97
Nobiletin	-6.08	-7.87	-7.86	-0.01	-1.34	1.79	-1.34
Positive control							
Verapamil	-6.66	-10.54	-9.88	-0.66	-1.81	3.88	-1.81
Nifedipine	-6.15	-7.94	-7.66	-0.29	-2.05	1.79	-2.05
Atorvastatin	-5.68	-10.26	-9.73	-0.53	-4.19	4.47	-4.19
Negative control (Non active)							
Captopril	-4.79	-6.28	-5.41	-0.87	-1.26	1.49	-1.26
Substrate							
Adenosine Triphosphate	-5.62	-10.09	-9.08	-1.01	-2.04	4.47	-2.04

Note: Estimated Free Energy of Binding (kcal/mol) = (1)+(2)+(3)-(4), (1) = (a)+(b), and (2) = (4)

ลิขสิทธิ์มหาวิทยาลัยเชียงใหม่
Copyright© by Chiang Mai University
All rights reserved

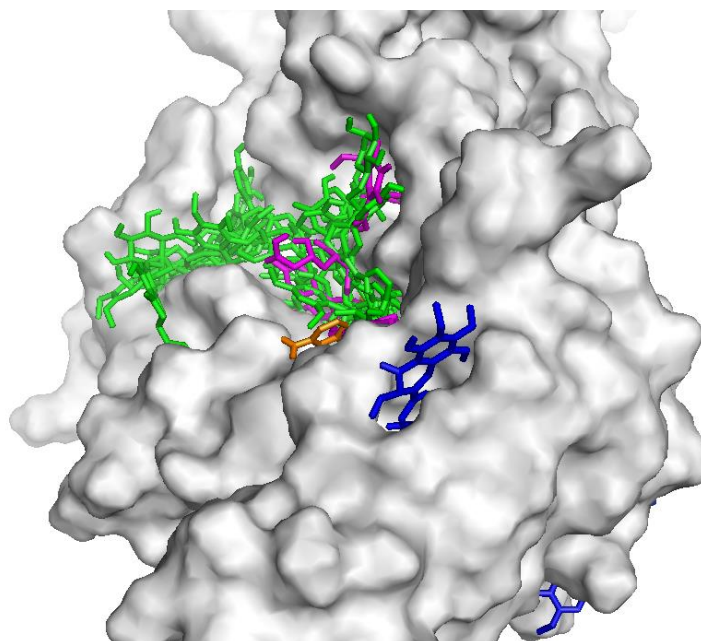


Figure 3.2 The binding patterns of the flavonoids on NBD1 of P-gp (white) visualised by PyMol. The binding cavity occupied by the most flavonoids (green), controls (magenta), and ATP (orange) is shown as a close-up inside NBD1 as the major binding site except 6a,12a-dehydroamorphigenin and 5HHMF (blue) bind NBD1 at their own distinct cavities

3.2.2 Correlation between experimental data and NBD1 docking scores

The result obtained from the docking study was supported by concordance with flavonoid percentage of inhibitory efficiency experimentally obtained (Table 3.4). $R^2 = 0.8711$ is shown in Figure 3.3. R^2 was obtained with a minimum of five points and R^2 values were higher than 0.6, a threshold routinely accepted to establish the goodness of structure-based models utilised in computational researches (Palmeira et al., 2012). This suggests that molecular docking approach to flavonoids using AutoDock at the ATP-binding site of NBD1 is powerful and capable to predict potential herb-drug interactions via P-gp among flavonoids and its drug substrates.

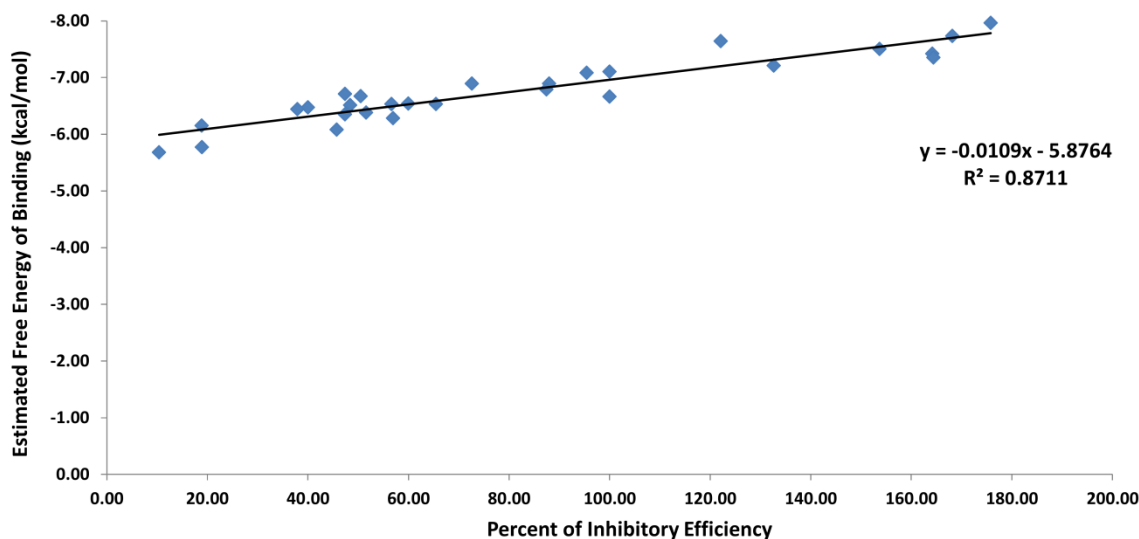


Figure 3.3 Correlation between docking scores (estimated free energies of binding) of flavonoids at NBD1 and percentage of inhibitory efficiency values

3.2.3 NBD1-based pharmacophore modelling (binding mode analysis) for P-gp–ligand interactions

Pharmacophore modelling for P-gp inhibitors was facilitated by the availability of 3D structural information on protein–ligand complexes. Molecular interactions of the ligands to any binding cavities at NBD1 were analysed from LigandScout’s output files in order to identify important features for ligand binding (Table 3.6). In Table 3.6, the structure-based pharmacophore models obtained from the docking complex illustrates the favourable binding position of flavonoids and controls with the lowest free energy of binding in the major active cavity of 4Q9H NBD1. 2D models show interactions between important amino acid residues and ligand formed in the cavities. Pharmacophore features in the models are colour-coded: green–hydrogen bond donor, red–hydrogen bond acceptor, yellow–hydrophobic interaction, blue–aromatic interaction, light blue–positive ionisable area and brown–negative ionisable area. Binding modes (Table 3.7).and major amino acid residues contributing P-gp–flavonoid interactions (Table 3.8) have been shown. Additionally, the crystal structures of P-gp including ligands were overlaid to illustrate ligand binding cavities (Figure 3.2).

At NBD1 (Figure 3.2), the important binding site inside NBD1 was observed. Regarding this site, it was a shallow cavity with an opened wide mount that was considered as the major binding site. The most flavonoids including all controls bound

to this site and the amino acid residues around the binding cavity including Asp160, His162, Val164, Tyr397, Ser430, Gln434, Gln437, Arg463, Ile466, Val468, Ser470, Gln471, Glu472, Pro473, Val474, Leu475, Gly521, Glu522, Ala525, Leu527, Lys532, Arg539, Ser555, Glu898, Asn899, Phe900, Arg901, Thr902, and Ser905 took responsibilities in hydrogen bond formations with the ligands; Ile156, Phe159, Val164, Tyr397, Val433, Leu439, Val468, Val474, Leu475, Val520, Ala536, Ala540, Ala556, Leu557, Thr902, and Leu906 took responsibilities in hydrophobic interactions with the ligands; Lys532, Thr902 and Leu906 took responsibilities in aromatic interactions with the ligands; and Asp160, and Asp551 took responsibilities in charge interactions with the ligands.

These amino acid residues of the major binding site played a key role in the molecular interactions with the most flavonoids and together with all controls. The interaction patterns of these most flavonoids as P-gp inhibitors corresponded with that of the drug P-gp inhibitors (positive controls) and ATP (a substrate control) as they occupied; (1) the same residues like Phe159, Asp160, Val164, Tyr397, Gln437, Leu439, Val468, Arg539, Ala540, Arg901, Thr902, Ser905, and Leu906 of positive controls and Ser430, Gln437, Ser470, Arg539, and Thr902 of ATP which is the natural substrate of P-gp NBD1 and (2) the same binding cavity of the positive controls and substrate at NBD1.

Additionally, in the bindings of 6a,12a-dehydroamorphigenin and 5-Hydroxy-3,6,7,8,3',4'-hexamethoxyflavone (5HHMF) with NBD1, ligand-transporter interactions occurred at their own distinct binding cavities. Regarding 6a,12a-dehydroamorphigenin, its binding site is quite far from the major binding site and only Met446 were responsible for hydrophobic interaction with the ligand. Regarding 5HHMF, its binding site is a wide mount pocket adjacent to the major binding site and only one interaction was formed by the hydrogen bond between Lys407 and the ligand. These van der Waals and polar forces were essential to support the interactions of two flavonoids in the active sites of NBD1.

Table 3.6 The structure-based pharmacophore models obtained from the docking complex illustrates in the major active cavity of 4Q9H NBD1

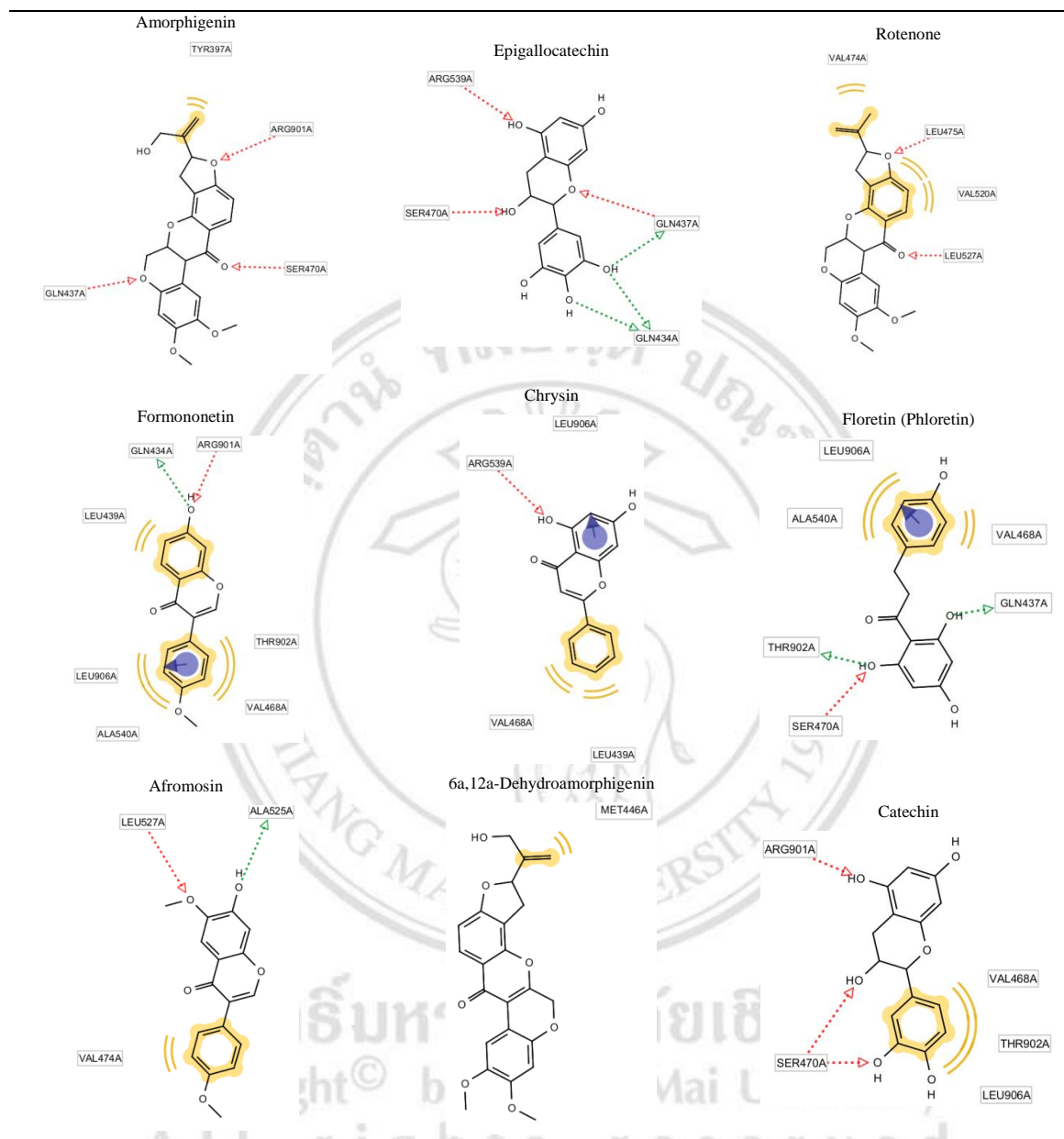


Table 3.6 (continued)

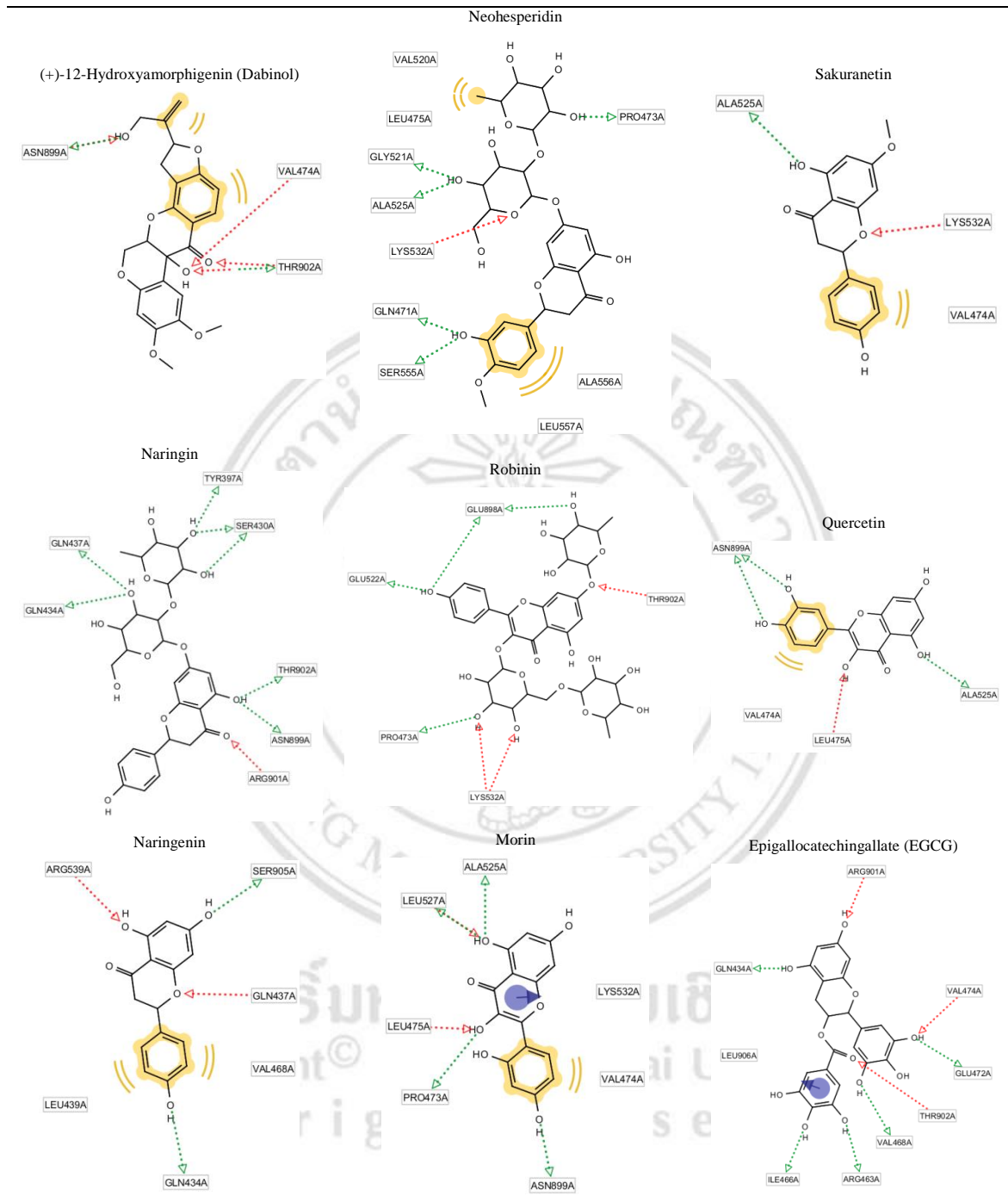


Table 3.6 (continued)

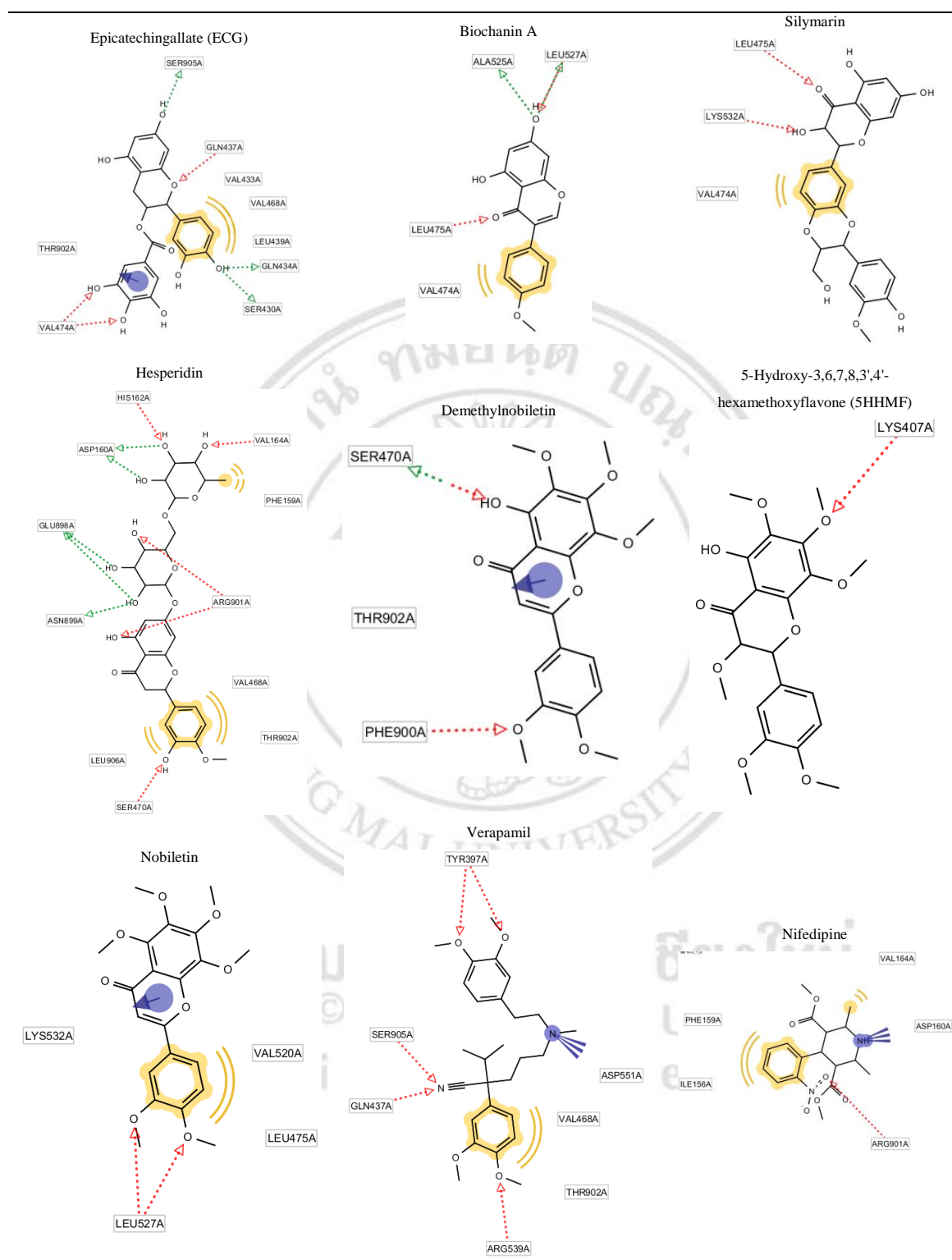


Table 3.6 (continued)

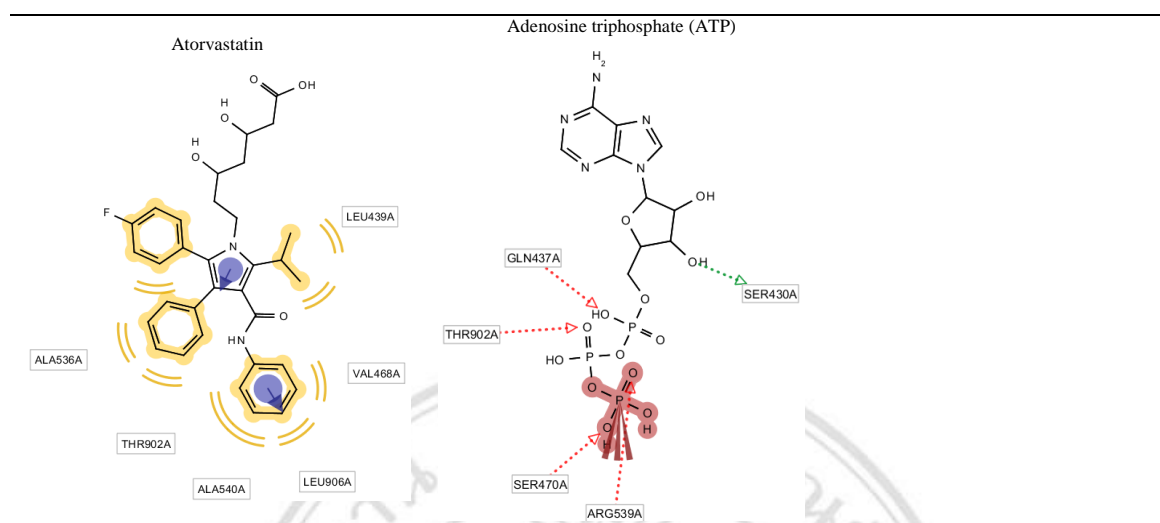


Table 3.7 Binding modes of flavonoids, control drugs, and substrate at NBD1

Compound	Residue involved in H-bond formation	Residue involved in hydrophobic interaction	Residue involved in aromatic interaction	Residue involved in Charge interaction
<i>Flavonoid</i>				
Amorphigenin	O (Ring B)–Gln437 O (Ring E)–Arg901 12-O–Ser470	Alkene side chain (Ring E)–Tyr397	-	-
Epigallocatechin	H (3'-OH)–Gln434 H (4'-OH)–Gln434 H (3'-OH)–Gln437 1-O–Gln437 O (3-OH)–Ser470 O (5-OH)–Arg539	-	-	-
Rotenone	O (Ring E)–Leu475 O (12-OH)–Leu527	Alkene side chain (Ring E)–Val474 Ring D–Leu475 Ring D–Val520	-	-
Formononetin	H (7-OH)–Gln434 O (7-OH)–Arg901	Ring A–Leu439 Ring B–Val468 Ring B–Ala540 Ring B–Thr902 Ring B–Leu906	Ring B–Leu906	-
Chrysin	O (5-OH)–Arg539	Ring B–Leu439 Ring B–Val468	Ring A–Leu906	-
Floretin (Phloretin)	H (1-OH)–Gln437 O (5-OH)–Ser470 H (5-OH)–Thr902	Aromatic side chain–Val468 Aromatic side chain–Ala540 Aromatic side chain–Leu906	Aromatic side chain–Leu906	-
Afromosin	H (7-OH)–Ala525 O (6-OCH ₃)–Leu527	Ring B–Val474	-	-
6a,12a-Dehydroamorphigenin	-	Alkene side chain (Ring E)–Met446	-	-
Catechin	O (5'-OH)–Ser470 O (3-OH)–Ser470 O (5-OH)–Arg901	Ring B–Val468 Ring B–Thr902 Ring B–Leu906	-	-

Table 3.7 (continued)

Compound	Residue involved in H-bond formation	Residue involved in hydrophobic interaction	Residue involved in aromatic interaction	Residue involved in Charge interaction
(+) -12-Hydroxyamorphigenin (Dabinol)	O(12a-OH)-Val474			
	O(OH side chain of Ring E)-Asn899			
	H (OH side chain of Ring E)-Asn899	Ring D-Val474		
	H-(12-OH)-Thr902	Alkene side chain (Ring E)-Val474	-	-
	O-(12-OH)-Thr902			
	H-(12a-OH)-Thr902			
	O-(12a-OH)-Thr902			
Neohesperidin	H (3'-OH)-Gln471			
	H (glycone)-Pro473	CH ₃ (glycone)-Leu475		
	H (glycone)-Gly521	CH ₃ (glycone)-Val520		
	H (glycone)-Ala525	Ring B-Ala556		
	O (glycone)-Lys532	Ring B-Leu557		
	H (3'-OH)-Ser555			
Sakuranetin	H (5-OH)-Ala525	Ring B-Val474	-	-
	1-O-Lys532			
Naringin	H (glycone)-Tyr397			
	H1 (glycone)-Ser430			
	H2 (glycone)-Ser430			
	H (glycone)-Gln434			
	H (glycone)-Gln437			
	H (5-OH)-Asn899			
	O (4-OH)-Arg901			
	H (5-OH)-Thr902			
Robinin	H (glycone)-Pro473			
	H (4'-OH)-Glu522			
	O (glycone)-Lys532			
	O (glycone)-Lys532			
	H (4'-OH)-Glu898			
	H (glycone)-Glu898			
	O (O-glycosidic bond)-Thr902			
Quercetin	O (3-OH)-Leu475			
	H (5-OH)-Ala525	Ring B-Val474		
	H (4'-OH)-Asn899			
	H (5'-OH)-Asn899			
Naringenin	H (4'-OH)-Gln434			
	1-O-Gln437	Ring B-Leu439		
	O (5-OH)-Arg539	Ring B-Val468		
	H (7-OH)-Ser905			
Morin	H (3-OH)-Pro473			
	O (3-OH)-Leu475			
	H (5-OH)-Ala525	Ring B-Val474	Ring C-Lys532	
	H (5-OH)-Leu527			
	O (5-OH)-Leu527			
	H (4'-OH)-Asn899			

Table 3.7 (continued)

Compound	Residue involved in H-bond formation	Residue involved in hydrophobic interaction	Residue involved in aromatic interaction	Residue involved in Charge interaction
Epigallocatechingallate (EGCG)	H (5'-OH)-Gln434			
	H (OH group of 3-Aromatic ring side chain)-Arg463			
	H (OH group of 3-Aromatic ring side chain)-Ile466		3-Aromatic ring side chain-Leu906	
	H (5'-OH)-Val468			
	H (3'-OH)-Glu472			
	O (3'-OH)-Val474			
	O (7-OH)-Arg901			
Epicatechingallate (ECG)	O (O of 3-Aromatic ring side chain)-Thr902			
	H (4'-OH)-Ser430			
	H (4'-OH)-Gln434			
	1-O-Gln437			
	1O (OH group of 3-Aromatic ring side chain)-Val474	Ring B-Val433	3-Aromatic ring side chain-Thr902	
	2O (OH group of 3-Aromatic ring side chain)-Val474	Ring B-Leu439		
		Ring B-Val468		
Biochanin A	H (7-OH)-Ser905			
	O (4-OH)-Leu475			
	H (7-OH)-Ala525	Ring B-Val474		
	H (7-OH)-Leu527			
Silymarin	O (7-OH)-Leu527			
	O (4-OH)-Leu475	Ring B-Val474		
Hesperidin	O (3-OH)-Lys532			
	H1 (OH of glycone)-Asp160			
	H2 (OH of glycone)-Asp160			
	O (OH of glycone)-His162	CH ₃ (glycone)-Phe159		
	O (OH of glycone)-Val164	CH ₃ (glycone)-Val164		
		Ring B-Val468		
		Ring B-Thr902		
		Ring B-Leu906		
Demethylnobiletin	O (5'-OH)-Ser470		Ring C-Thr902	
	O (5-OH)-Ser470			
	O (5-OCH ₃)-Phe900			
5-Hydroxy-3,6,7,8,3',4'-hexamethoxyflavone (5HHMF)	O (7-OCH ₃)-Lys407			
Nobiletin	O (4'-OCH ₃)-Leu527	Ring B-Leu475	Ring C-Lys532	
	O (5'-OCH ₃)-Leu527	Ring B-Val520		

Table 3.7 (continued)

Compound	Residue involved in H-bond formation	Residue involved in hydrophobic interaction	Residue involved in aromatic interaction	Residue involved in Charge interaction
<i>Positive control</i>				
Verapamil (Strong inhibitor)	1-O (OCH ₃)–Tyr397			
	2-O (OCH ₃)–Tyr397			
	N–Gln437	Benzene ring–Val468	-	N–Asp551
	3-O (OCH ₃)–Arg539 N–Ser905	Benzene ring–Thr902		
Nifedipine	O–Arg901	Benzene ring–Ile156		
		Benzene ring–Phe159 CH ₃ –Val164	-	N (secondary amine)– Asp160
Atorvastatin		CH-CH ₃ side chain–Leu439		
		CH-CH ₃ side chain–Val468		
		Benzene ring–Val468		
		Benzene ring–Ala536		
		Benzene ring–Ala540	Pyrrole ring–Thr902	
		Benzene ring1–Thr902	Benzene ring–Leu906	
		Benzene ring2–Thr902		
		Benzene ring3–Thr902 Benzene ring–Leu906		
<i>Substrate</i>				
Adenosine triphosphate (ATP)	H (OH side chain)–Ser430			
	O (phosphate group)– Gln437			
	O (phosphate group)– Ser470			
	O (phosphate group)– Arg539			
	O (phosphate group)– Thr902			

Table 3.8 The important amino acid residues of NBD1 that involved in the molecular interactions of P-gp crystal structures (4Q9H) with its inhibitors (flavonoids) identified by LigandScout

Amino acid residue	Number of H-bond involved (Number of compound involved)	Number of hydrophobic interaction involved (Number of compound involved)	Number of aromatic interaction involved (Number of compound involved)	Number of charge interaction involved (Number of compound involved)
Phe159 ^a	-	1 (1)	-	-
Asp160 ^a	2 (1)	-	-	-
His162	1 (1)	-	-	-
Val164 ^a	1 (1)	1 (1)	-	-
Tyr397 ^a	1 (1)	1 (1)	-	-
Lys407	1 (1)	-	-	-
Ser430 ^b	3 (2)	-	-	-
Val433	-	1 (1)	-	-
Gln434	7 (6)	-	-	-
Gln437 ^{a,b}	7 (6)	-	-	-
Leu439 ^a	-	4 (4)	-	-
Met446	-	1 (1)	-	-
Arg463	1 (1)	-	-	-
Ile466	1 (1)	-	-	-
Val468 ^a	1 (1)	7 (7)	-	-
Ser470 ^b	8 (6)	-	-	-
Gln471	1 (1)	-	-	-
Glu472	1 (1)	-	-	-
Pro473	3 (3)	-	-	-
Val474	4 (3)	9 (8)	-	-
Leu475	5 (5)	2 (2)	-	-
Val520	-	3 (3)	-	-
Gly521	1 (1)	-	-	-
Glu522	1 (1)	-	-	-
Ala525	6 (6)	-	-	-
Leu527	8 (5)	-	-	-
Lys532	5 (4)	-	2 (2)	-
Arg539 ^{a,b}	3 (3)	-	-	-
Ala540 ^a	-	2 (2)	-	-
Ser555	1 (1)	-	-	-
Ala556	-	1 (1)	-	-
Leu557	-	1 (1)	-	-
Glu898	4 (2)	-	-	-
Asn899	7 (5)	-	-	-
Phe900	1 (1)	-	-	-
Arg901 ^a	7 (6)	-	-	-
Thr902 ^{a,b}	8 (5)	3 (3)	2 (2)	-
Ser905 ^a	2 (2)	-	-	-
Leu906 ^a	-	4 (4)	4 (4)	-

^aAmino acid residues that interact with the positive controls.
^bAmino acid residues that interact with ATP.

3.2.4 Docking of P-gp inhibiting compounds against NBD2

Docking of the 25 flavonoids against NBD2 was conducted. The optimal pose of each compound with the lowest estimated free energy of binding ranging from -7.74 to -5.39 kcal/mol were then used for further linear regression analysis. Notably, the more negative the estimated free energy of binding value was, the tighter the predicted value was. 8 flavonoids (amorphigenin, epigallocatechin, rotenone, formononetin, chrysin,

epigallocatechingallate, biochanin A, and hesperidin) exhibited *in vitro* strong P-gp inhibitory activity showed low estimated free energy of binding values ranging from -7.74 to -6.93 kcal/mol. Other 17 flavonoids exhibited *in vitro* active (weak) P-gp inhibitory activity had relatively higher estimated free energy of binding values ranging from -7.05 to -5.39 kcal/mol. 3 known P-gp inhibitors (verapamil, nifedipine, and atorvastatin) used as positive controls, 1 non P-gp inhibitor (captopril), and 1 P-gp substrate (ATP) also were conducted docking. It was shown that verapamil which is a strong inhibitor of P-gp was of low estimated free energy of binding (-6.97 kcal/mol); and the moderate P-gp inhibitor (nifedipine) and the weak P-gp inhibitor (atorvastatin) were of relatively higher energies (-5.83 and -5.56 kcal/mol respectively). The inhibition of flavonoids on the metabolism of ATP depended on whether their free energies of binding were much lower than that of ATP or not. The estimated free energy of binding of natural substrate of P-gp (ATP) was -5.27 kcal/mol which was considered to be the threshold of positive binding and the estimated free energy of binding of all the test compounds was much lower than -5.27 kcal/mol, showing that they all can bind to the catalytic site of NBD2 (Table 3.9). Regarding the non P-gp inhibitor; captopril, it was of the lowest binding affinity to NBD2 of P-gp with the highest docking score -4.70 kcal/mol. Table 3.10 illustrates the complete profile of parameters of free energy of binding as final intermolecular energy, total estimated energy of vdW+Hbond+desolv, electrostatic energy, final total internal energy, torsional free energy, and unbound system's energy were evaluated to estimate the favourable binding of all flavonoids and controls for their interaction with NBD2. A calculation of estimated free energy of binding of each flavonoid from these parameters is shown under the table.

Copyright © by Chiang Mai University
All rights reserved

Table 3.9 The experimental P-gp inhibitory activity value expressed by percentage compared to a positive control (verapamil) and the docking score at NBD2 expressed by the estimated free energy of binding of each flavonoid

Flavonoid	Inhibitory efficiency unit	Percentage of activity compared to a positive control (verapamil)	Estimated Lowest Free Energy of Binding in Cluster (kcal/mol)	Estimated Inhibition Constant of the Selected Docking Pose, K_i (μ M)	Classification (by observed inhibitory activity)
<i>pFAR^a</i>					
Amorphigenin	-1.67	175.79	-7.74	2.13	Strong
Epigallocatechin	-1.56	164.21	-7.23	5.08	Strong
Rotenone	-1.46	153.68	-7.30	4.47	Strong
Formononetin	-1.26	132.63	-7.24	4.97	Strong
Chrysin	-1.16	122.11	-6.99	7.56	Strong
Floretin (Phloretin)	-0.69	72.63	-6.40	20.33	Active
Afrososin	-0.49	51.58	-6.18	46.22	Active
6a,12a-Dehydroamorphigenin	-0.48	50.53	-6.22	8.86	Active
Catechin	-0.46	48.42	-6.22	93.48	Active
(+)-12-Hydroxyamorphigenin (Dabinol)	-0.45	47.37	-6.21	28.26	Active
Neohesperidin	-0.45	47.37	-5.70	66.33	Active
Sakuranetin	-0.38	40.00	-5.93	44.78	Active
Naringin	-0.36	37.89	-5.82	53.81	Active
Robinin	-0.18	18.95	-5.39	112.72	Active
Verapamil	-0.95	100	-6.97	7.84	Strong (positive control)
<i>% of negative control on [³H]-daunomycin accumulation in MCF-7/ADR cells^b</i>					
Quercetin	201.8 \pm 16.4%	87.97	-7.05	6.76	Active
Naringenin	130.6 \pm 0.9%	56.93	-6.56	15.48	Active
Morin	129.9 \pm 2.6%	56.63	-6.27	25.28	Active
Verapamil	229.4 \pm 17.6%	100	-6.97	7.84	Strong (positive control)
<i>Accumulation ratio of rhodamine-123 in KB-C2 cells^c</i>					
Epigallocatechingallate (EGCG)	3.7	168.18	-7.57	2.81	Strong
Epicatechingallate (ECG)	2.1	95.45	-7.05	6.81	Active
Verapamil	2.2	100	-6.97	7.84	Strong (positive control)
<i>% of negative control on [³H]-daunomycin accumulation in MCF-7/ADR cells^d</i>					
Biochenin A	300	100	-6.93	8.31	Strong
Silymarin	180	60	-6.40	20.33	Active
Verapamil	300	100	-6.97	7.84	Strong (positive control)

Table 3.9 (continued)

Flavonoid	Inhibitory efficiency unit	Percentage of activity compared to a positive control (verapamil)	Estimated Lowest Free Energy of Binding in Cluster (kcal/mol)	Estimated Inhibition Constant of the Selected Docking Pose, K_i (μM)	Classification (by observed inhibitory activity)
<i>Inhibition efficiency (already converted from Fluorescence intensity of rhodamine123)^e</i>					
Hesperidin	164.41 \pm 11.00	164.41 \pm 11.00	-7.45	3.48	Strong
Demethylnobiletin	87.43 \pm 20.45	87.43 \pm 20.45	-6.88	9.06	Active
5-Hydroxy-3,6,7,8,3',4'-hexamethoxyflavone (SHHMF)	65.47 \pm 13.16	65.47 \pm 13.16	-6.61	14.25	Active
Nobiletin	45.71 \pm 7.49	45.71 \pm 7.49	-5.90	16.8	Active
Verapamil	100.00 \pm 4.98	100.00 \pm 4.98	-6.97	7.84	Strong (positive control)
Positive control					
<i>In vitro IC₅₀^f</i>					
Verapamil	10 μM	100	-6.97	7.84	Strong
Nifedipine	53 μM	18.87	-5.83	53.93	Moderate
Atorvastatin	96 μM	10.42	-5.56	83.42	Weak
Negative control					
Captopril	>1,000 μM	0	-4.70	361.52	Non active
Substrate					
Adenosine Triphosphate	-	-	-5.27	137.09	-

^a = (Gyémant et al., 2005; Martins et al., 2010), ^b = (Chung et al., 2005), ^c = (Kitagawa et al., 2004), ^d = (Zhang & Morris, 2003), ^e = (El-Readi et al., 2010), ^f = (Fenner et al., 2009)

ลิขสิทธิ์มหาวิทยาลัยเชียงใหม่
Copyright© by Chiang Mai University
All rights reserved

Table 3.10 Composition of docking energy against NBD2 of each flavonoid

Flavonoid	Estimated Lowest Free Energy of Binding in Cluster (kcal/mol)	Final Intermolecular Energy (kcal/mol) (1)	vdW + Hbond + desolv Energy (kcal/mol) (a)	Electrostatic Energy (kcal/mol) (b)	Final Total Internal Energy (kcal/mol) (2)	Torsional Free Energy (kcal/mol) (3)	Unbound System's Energy (kcal/mol) (4)
Amorphigenin	-7.74	-9.23	-9.07	0.16	-0.29	1.49	-0.29
Epigallocatechin	-7.23	-9.31	-8.65	-0.66	-2.26	2.09	-2.26
Rotenone	-7.30	-8.19	-8.18	-0.01	-0.32	0.89	-0.32
Formononetin	-7.24	-8.13	-7.93	-0.2	-0.35	0.89	-0.35
Chrysin	-6.99	-7.88	-7.78	-0.1	-0.95	0.89	-0.95
Floretin (Phloretin)	-6.40	-8.79	-8.53	-0.25	-1.06	2.39	-1.06
Afromosin	-6.18	-7.11	-6.8	-0.31	-0.72	1.19	-0.72
6a,12a-Dehydroamorphigenin	-6.22	-8.38	-8.29	-0.1	-0.4	1.49	-0.4
Catechin	-6.22	-7.29	-7.09	-0.2	-2.25	1.79	-2.25
(+)-12-Hydroxyamorphigenin (Dabinal)	-6.21	-8.0	-7.85	-0.15	-1.37	1.79	-1.37
Neohesperidin	-5.70	-10.17	-10.15	-0.02	-8.11	4.47	-8.11
Sakuranetin	-5.93	-7.13	-6.97	-0.15	-1.02	1.19	-1.02
Naringin	-5.82	-10.0	-9.96	-0.04	-6.22	4.18	-6.22
Robinin	-5.39	-11.05	-10.55	-0.5	-9.21	5.67	-9.21
Quercetin	-7.05	-8.84	-8.53	-0.31	-2.83	1.79	-2.83
Naringenin	-6.56	-7.76	-7.65	-0.11	-0.95	1.19	-0.95
Morin	-6.27	-8.06	-7.87	-0.2	-2.12	1.79	-2.12
Epigallocatechingallate (EGCG)	-7.57	-11.15	-10.85	-0.31	-4.96	3.58	-4.96
Epicatechingallate (ECG)	-7.05	-10.33	-9.96	-0.37	-4.37	3.28	-4.37
Biochenin A	-6.93	-8.12	-8.04	-0.09	-0.91	1.19	-0.91
Silymarin	-6.40	-9.09	-8.62	-0.47	-3.96	2.68	-3.96
Hesperidin	-7.45	-11.92	-11.97	0.05	-4.37	4.47	-4.37
Demethylnobiletin	-6.88	-8.97	-8.65	-0.32	-1.91	2.09	-1.91
5-Hydroxy-3,6,7,8,3',4'-hexamethoxyflavone (5HHMF)	-6.61	-8.7	-8.55	-0.15	-2.04	2.09	-2.04
Nobiletin	-5.09	-8.6	-8.17	-0.43	-1.47	2.09	-1.47
Positive control							
Verapamil	-6.97	-10.84	-10.43	-0.41	-1.61	3.88	-1.61
Nifedipine	-5.83	-7.62	-6.18	-1.44	-1.82	1.79	-1.82
Atorvastatin	-5.56	-10.04	-9.47	-0.57	-3.24	4.47	-3.24
Negative control (Non active)							
Captopril	-4.70	-6.19	-5.38	-0.8	-0.94	1.49	-0.94
Substrate							
Adenosine Triphosphate	-5.27	-9.74	-9.58	-0.17	-3.15	4.47	-3.15

Note: Estimated Free Energy of Binding (kcal/mol) = (1)+(2)+(3)-(4), (1) = (a)+(b), and (2) = (4)

ลิขสิทธิ์มหาวิทยาลัยเชียงใหม่
Copyright© by Chiang Mai University
All rights reserved

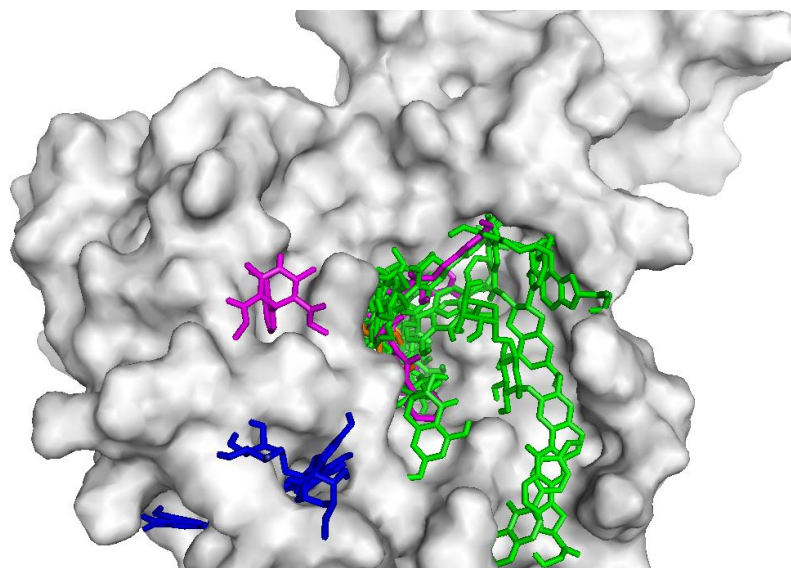


Figure 3.4 The binding patterns of the inhibitors on NBD2 of P-gp (white). The binding cavity occupied by the most flavonoids (green), controls (magenta) and ATP (orange) is shown as a close-up inside NBD2 as the major binding site. Formononetin, chrysin, catechin, naringin, and naringenin (blue) bind NBD2 at another pocket as the minor binding site

3.2.5 Correlation between experimental data and NBD2 docking scores

The result obtained from the docking study was supported by concordance with flavonoid percentage of inhibitory efficiency experimentally obtained (Table 3.9). $R^2 = 0.8941$ is shown in Figure 3.5. R^2 was obtained with a minimum of five points and R^2 values were higher than 0.6, a threshold routinely accepted to establish the goodness of structure-based models utilised in computational researches (Palmeira et al., 2012). This suggests that molecular docking approach to flavonoids using AutoDock at the ATP-binding site of NBD2 is powerful and capable to predict potential herb-drug interactions via P-gp among flavonoids and its drug substrates.

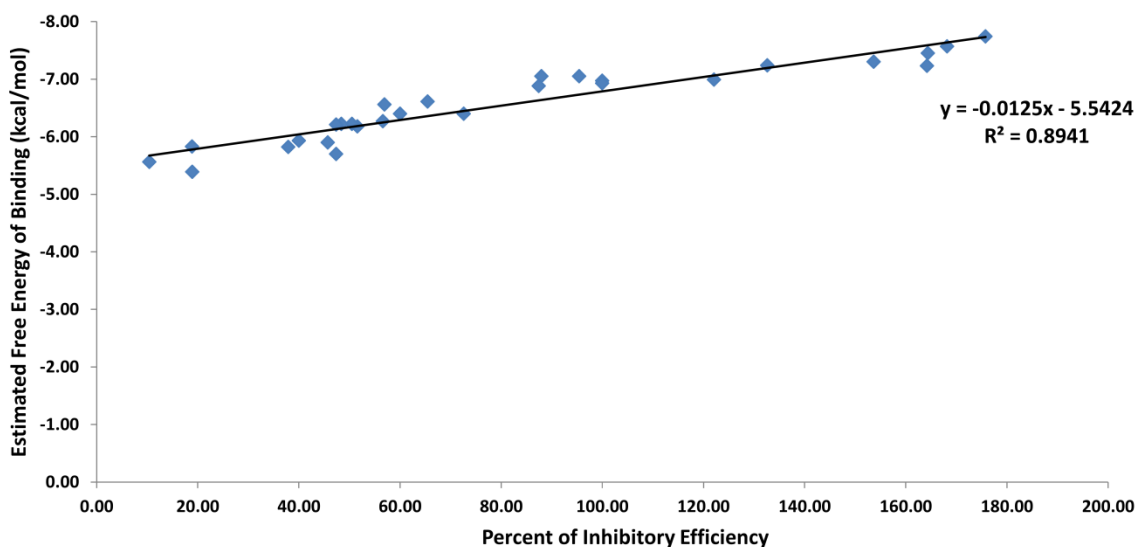


Figure 3.5 Correlation between docking scores (estimated free energies of binding) of flavonoids at NBD2 and percentage of inhibitory efficiency values

3.2.6 NBD2-based pharmacophore modelling (binding mode analysis) for P-gp–ligand interactions

Pharmacophore modelling for P-gp inhibitors was facilitated by the availability of 3D structural information on protein–ligand complexes. Molecular interactions of the ligands to any binding cavities at both NBDs were analysed from LigandScout’s output files in order to identify important features for ligand binding (Table 3.11). In Table 3.11, the structure-based pharmacophore models obtained from the docking complex illustrates the favourable binding position of flavonoids and controls with the lowest free energy of binding in the major active cavity of 4Q9H NBD2. 2D models show interactions between important amino acid residues and ligand formed in the cavities. Pharmacophore features in the models are colour-coded: green–hydrogen bond donor, red–hydrogen bond acceptor, and yellow–hydrophobic interaction, and blue–aromatic interaction, and brown–positive ionisable area. Binding modes (Table 3.12).and major amino acid residues contributing P-gp–flavonoid interactions (Table 3.13) have been shown. Additionally, the crystal structures of P-gp including ligands were overlaid to illustrate ligand binding cavities (Figure 3.4).

The characteristic of NBD2 was quite different from NBD1. At NBD2 (Figure 3.4), two important binding sites inside NBD2 were observed. Regarding the first binding site, it was a shallow cavity with an opened wide mount (as same as the major

binding site of NBD1) that was considered as the major binding site. The most flavonoids and all controls bound to this site and the amino acid residues around the binding cavity including Leu254, Ala255, Arg258, Thr259, Phe800, Asp801, Asp802, Thr806, Thr807, Tyr1040, Arg1043, Ser1067, Gly1069, Cys1070, Gly1071, Ser1073, Val1076, Gln1077, Glu1080, Ile1111, Ser1113, Gln1114, Glu1115, Ile1117, Gly1174, Arg1184, Asp1196, Glu1197, Ile1242, and Asn1244 took responsibilities in hydrogen bond formations with the ligands; Ala255, Ile257, Thr259, Ala262, Phe263, Thr807, Thr1042, Ile1046, Val1048, Val1076, Phe1082, Ile1111, Ile1117, Ala1181, and Ala1201 took responsibilities in hydrophobic interactions with the ligands; Arg258, and Arg1184 took responsibilities in aromatic interactions with the ligands; and Arg258 took responsibilities in charge interaction with the ligand.

These amino acid residues of the major binding site played key roles in ligand–transporter interactions with the most flavonoids and together with all controls. The interaction patterns of these most flavonoids as P-gp inhibitors corresponded with that of the most drug P-gp inhibitors (positive controls) and ATP (a substrate control) as they occupied; (1) the same residues like Ala255, Ile257, Arg258, Thr259, Ala262, Phe263, Thr806, Thr807, Val1076, Ile1111, Glu1115, and Ile1117 of positive controls and Ser1113, Gln1114, Glu1115, Ile1117, and Arg1184 of ATP which is the natural substrate of P-gp NBD2 and (2) the same binding cavity (the major binding site) of the positive controls and substrate at NBD2.

The second binding site was a deep narrow hydrophobic pocket with a wide hydrophilic mount that was considered as the minor binding site. It located closely to the major one. Formononetin, chrysin, catechin, naringin, and naringenin bound to this site and the amino acid residues of the binding pocket including Gln1114, Glu1197, Ser1200, Leu1202, Glu1207, Lys1208, Gln1211, Leu1214, Arg1218, His1228, Arg1229, and Asn1235 took responsibilities in hydrogen bond formations with the ligands around the pocket mount, and Leu1195, Ala1198, Thr1199, Leu1214, Val1225, Ala1227, Thr1232, and Ile1233 took responsibilities in hydrophobic interactions with the ligands inside the pocket. The interaction pattern of chrysin corresponded with that of ATP as it occupied the same amino acid residue like Gln1114 of ATP which is a key residue of the major binding site.

These polar and van der Waals forces were essential to support the interactions of these flavonoids in the active sites of NBD2.

Table 3.11 The structure-based pharmacophore models obtained from the docking complex illustrates in the major active cavity of 4Q9H NBD2.

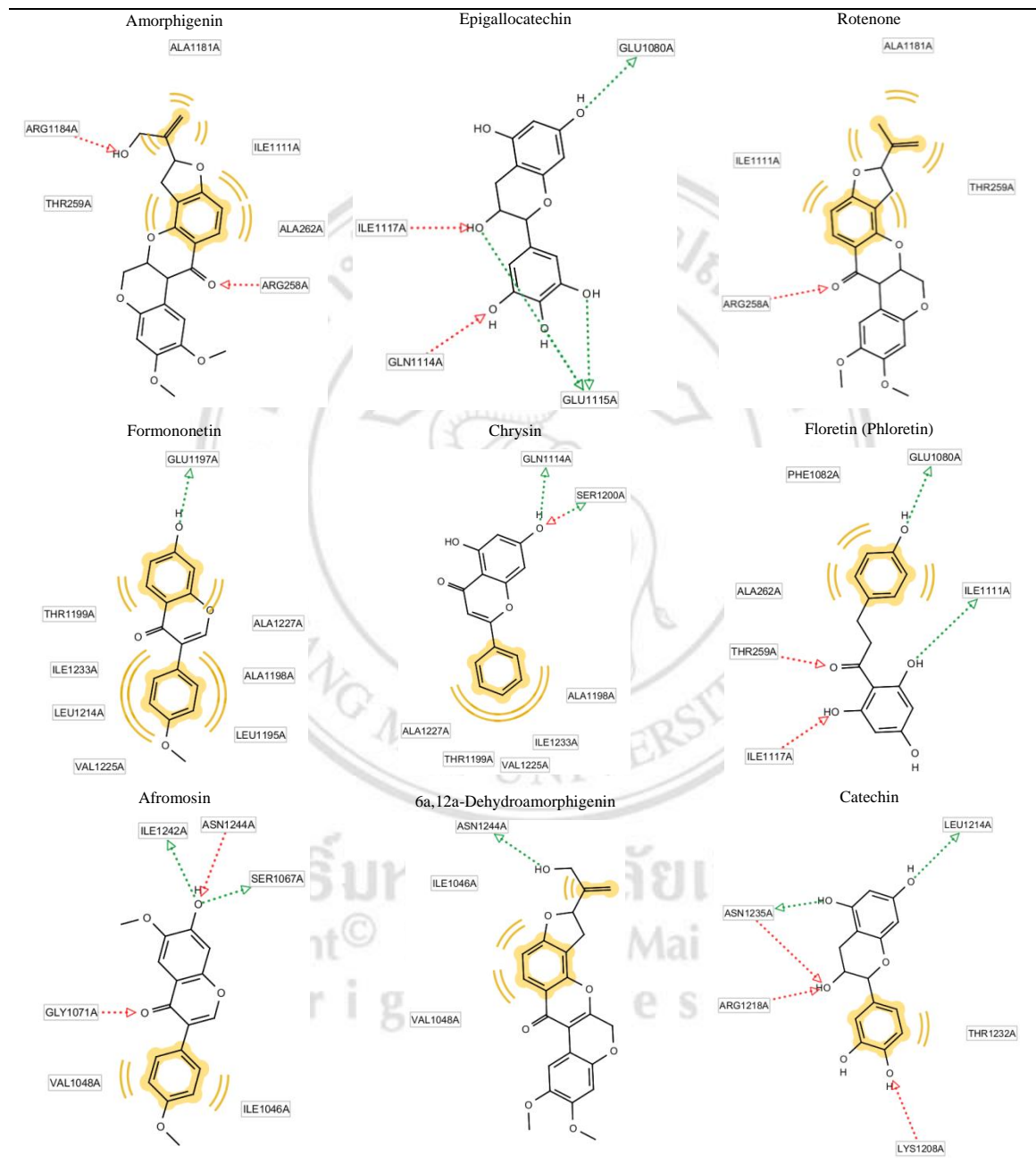


Table 3.11 (continued)

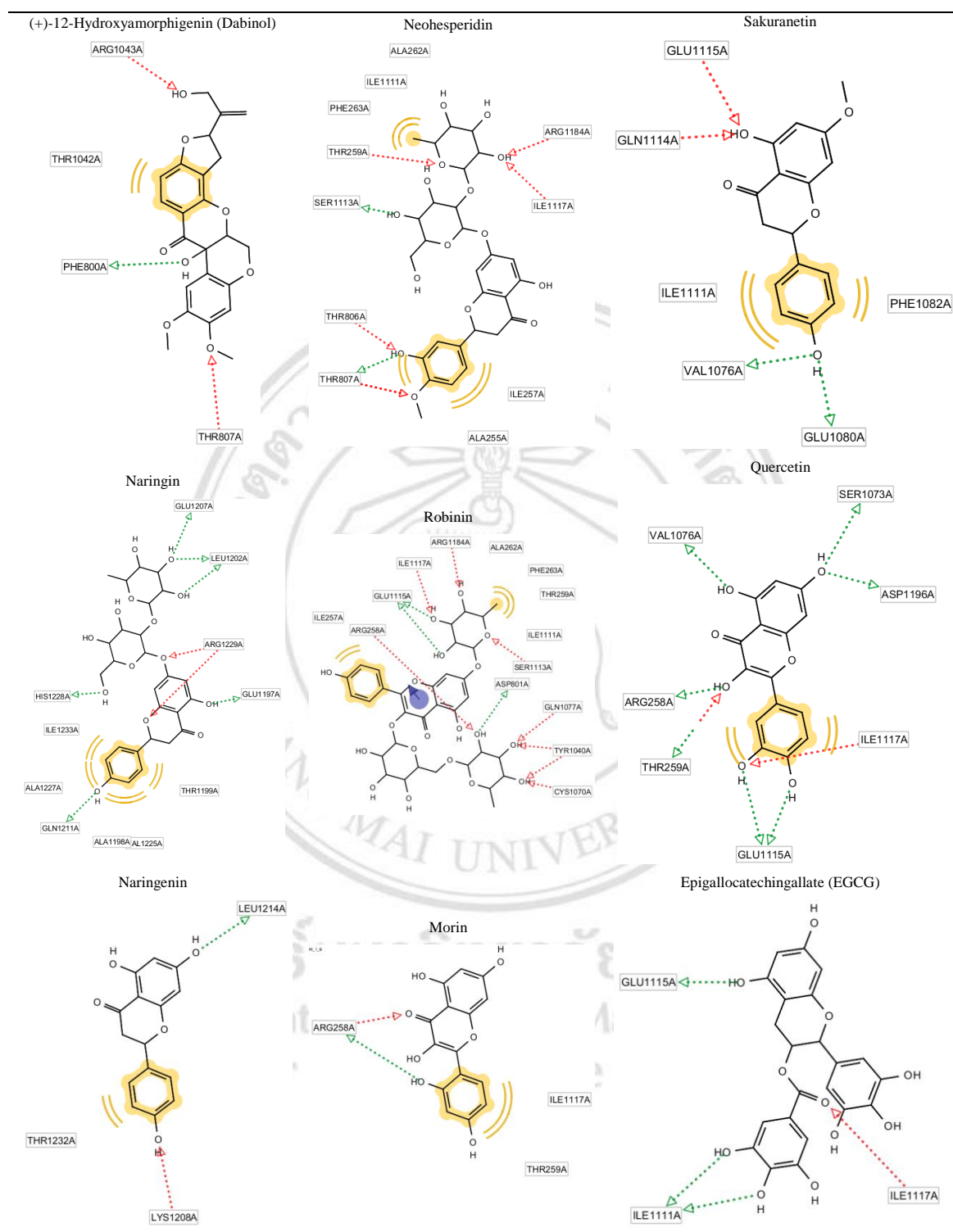
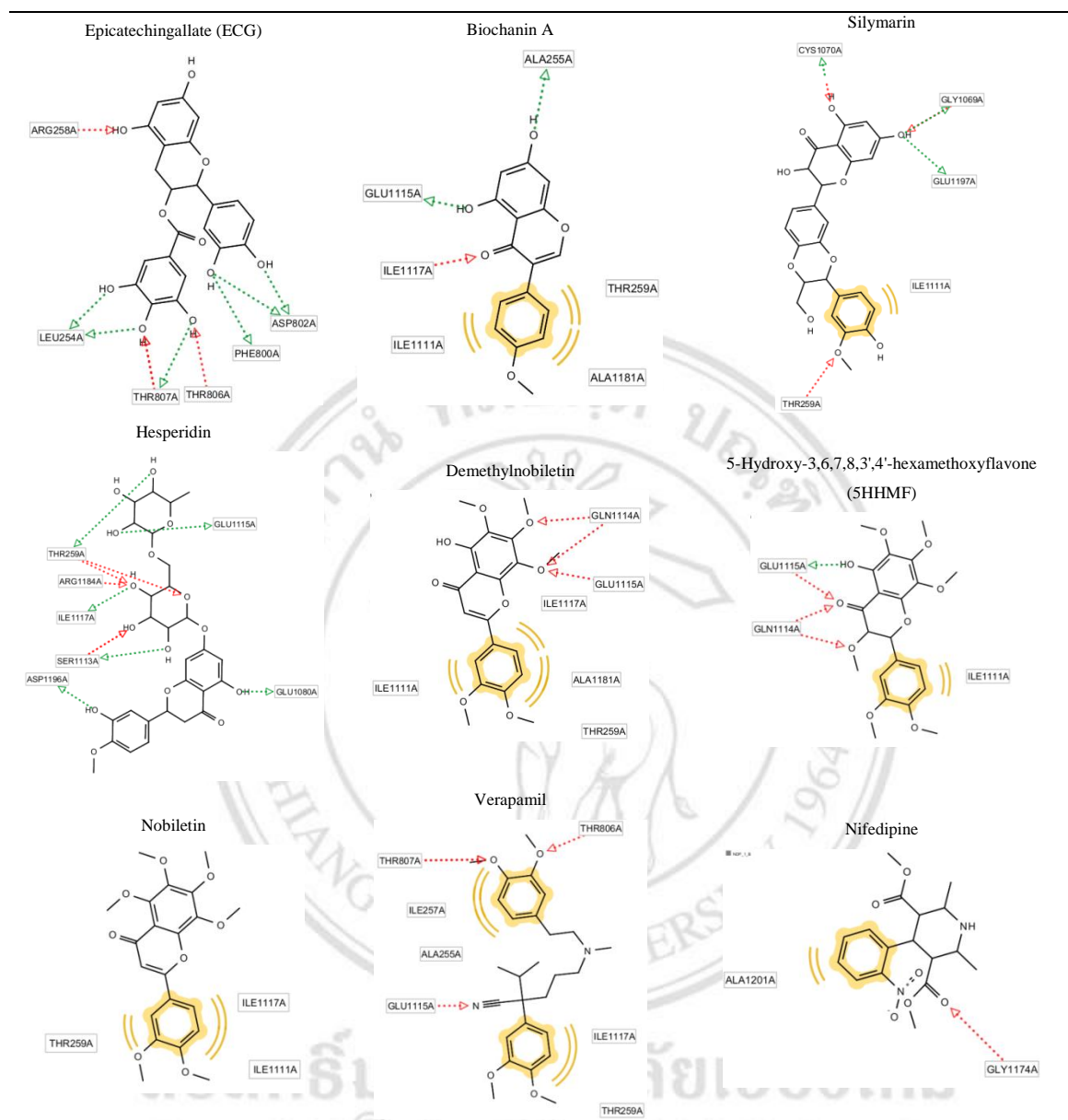


Table 3.11 (continued)



Copyright © by Chiang Mai University
All rights reserved

Table 3.11 (continued)

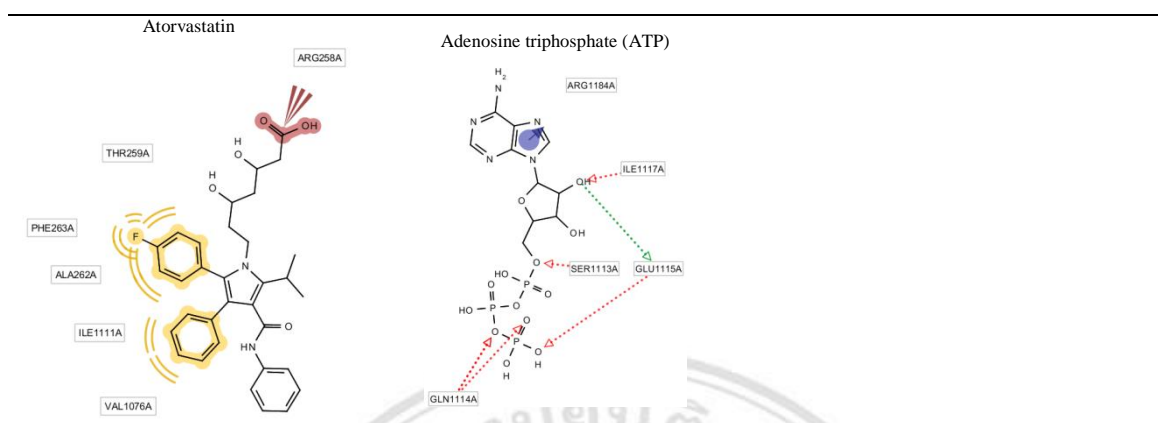


Table 3.12 Binding modes of flavonoids, control drugs, and substrate at NBD2

Compound	Residue involved in H-bond formation	Residue involved in hydrophobic interaction	Residue involved in aromatic interaction	Residue involved in Charge interaction
<i>Flavonoid</i>				
Amorphenigenin	O (12-OH)-Arg258 O (OH side chain of Ring E)-Arg1184	CH-CH ₃ side chain (Ring E)-Thr259 Ring D-Ala262 CH-CH ₃ side chain (Ring E)-Ile1111 CH-CH ₃ side chain (Ring E)-Ala1181 Ring D-Ile1111	-	-
Epigallocatechin	H (7-OH)-Glu1080 O (5'-OH)-Gln1114 H (3-OH)-Glu1115 H (3'-OH)-Glu1115 O (3-OH)-Ile1117	-	-	-
Rotenone	O (12-OH)-Arg258	2 CH-CH ₃ (Ring E)-Thr259 2 CH-CH ₃ (Ring E)-Ile1111 2 CH-CH ₃ (Ring E)-Ala1181 Ring D-Thr259 Ring D-Ile1111	-	-
Formononetin	H (7-OH)-Glu1197	Ring A-Thr1199 Ring A-Ala1227 Ring B-Leu1195 Ring B-Ala1198 Ring B-Leu1214 Ring B-Val1225 Ring B-Ile1233 Ring B-Ala1198	-	-
Chrysin	H (7-OH)-Gln1114 H (7-OH)-Ser1200 O (7-OH)-Ser1200	Ring B-Thr1199 Ring B-Val1225 Ring B-Ala1227 Ring B-Ile1233	-	-

Table 3.12 (continued)

Compound	Residue involved in H-bond formation	Residue involved in hydrophobic interaction	Residue involved in aromatic interaction	Residue involved in Charge interaction
Floretin (Phloretin)	O (4-O)-Thr259			
	H (OH of aromatic side chain)-Glu1080	Aromatic side chain-Ala262 Aromatic side chain-Phe1082	-	-
	H (1-H)-Ile1111	Aromatic side chain-Ile1111		
	O (5-OH)-Ile1117			
Afromosin	H (7-OH)-Ser1067			
	H (7-OH)-Ile1242	Ring B-Ile1046		
	O (7-OH)-Asn1244	Ring B- Val1048	-	-
	O (7-OH)-Gly1071			
6a,12a-Dehydroamorphigenin		CH-CH ₃ side chain (Ring E)- Ile1046		
	O (OH side chain of ring E)- Asn1244	Ring D-Ile1046	-	-
		Ring D-Val1048		
Catechin	O (4'-OH)-Lys1208			
	H (7-OH)-Leu1214			
	O (3-OH)-Arg1218	Ring B-Thr1232		
	H (5-OH)-Asn1235			
	O (3-OH)- Asn1235			
(+)12-Hydroxyamorphigenin (Dabinol)	H-(12a-OH)-Phe800			
	O (3-OCH ₃)-Thr807	Ring D-Thr1042	-	-
	O (OH side chain of Ring E)- Arg1043			
Neohesperidin	O (glycone)-Thr259			
	O (3'-OH)-Thr806	Ring B-Ala255		
	H (3'-OH)-Thr807	Ring B-Ile257		
	O (4'-OCH ₃)-Thr807	CH ₃ (glycone)-Phe263		
	H (glycone)-Ser1113	Ring B-Thr807		
	O (glycone)-Ile1117	CH ₃ (glycone)-Ile1111		
	O (glycone)-Arg1184			
Sakuranetin	H (4'-OH)-Val1076	Ring B-Val1076		
	H (4'-OH)-Glu1080	Ring B-Phe1082	-	-
	O (5-OH)-Gln1114	Ring B-Ile1111		
	O (5-OH)-Glu1115			
Naringin	H (5-OH)-Glu1197			
	H1 (glycone)-Leu1202	Ring B-Ala1198		
	H2 (glycone)-Leu1202	Ring B-Thr1199		
	H (glycone)-Glu1207	Ring B-Val1225		
	H (4'-OH)-Gln1211	Ring B-Ala1227		
	H (glycone)-His1228	Ring B-Ile1233		
	O (glycosidic bond)-Arg1229 1-O-Arg1229			
Robinin	O (glycone)-Arg258			
	H (glycone)-Asp801			
	O1 (glycone)-Tyr1040			
	O2 (glycone)-Tyr1040	Ring B-Ile257		
	O (glycone)-Cys1070	CH ₃ of glycone-Thr259	Ring C-Arg258	
	O (glycone)-Gln1077	CH ₃ of glycone-Ala262		
	O (glycone)-Ser1113	CH ₃ of glycone-Phe263		
	H1 (glycone)-Glu1115			
	H2 (glycone)-Glu1115			
	O (glycone)-Ile1117			
O (glycone)-Arg1184				

Table 3.12 (continued)

Compound	Residue involved in H-bond formation	Residue involved in hydrophobic interaction	Residue involved in aromatic interaction	Residue involved in Charge interaction
Quercetin	H (3-OH)-Arg258			
	H (3-OH)-Thr259			
	O (3-OH)-Thr259			
	H (7-OH)-Ser1073	Ring B-Thr259		
	H (5-OH)-Val1076	Ring B-Ile1117	-	-
	H (4'-OH)-Glu1115			
	H (5'-OH)-Glu1115			
	O (5'-OH)-Ile1117			
Naringenin	H (7-OH)-Asp1196			
	O (4'-OH)-Lys1208	Ring B-Thr1232	-	-
Morin	H (7-OH)-Leu1214	Ring B-Thr259		
	H (6'-OH)-Arg258	Ring B-Ile1117	-	-
Epigallocatechingallate (EGCG)	O (4-OH)-Arg258			
	H1 (3-side chain)-Ile1111			
	H2 (3-side chain)-Ile1111			
	H (5-OH)-Glu1115			
Epicatechingallate (ECG)	O (3-side chain)-Ile1117			
	H1 (3-side chain)-Leu254			
	H2 (3-side chain)-Leu254			
	O (5-OH)-Arg258			
	H (5'-OH)-Phe800			
	H (4'-OH)-Asp802			
	H (5'-OH)-Asp802			
	O (3-side chain)-Thr806			
	H (3-side chain)-Thr807			
O (3-side chain)-Thr807				
Biochanin A	H (7-OH)-Ala255	Ring B-Thr259		
	H (5-OH)-Glu1115	Ring B-Ile1111	-	-
	O (4-OH)-Ile1117	Ring B-Ala1181		
Silymarin	O (5'-OCH ₃)-Thr259			
	H (7-OH)-Gly1069			
	O (7-OH)-Gly1069	Aromatic ring-Ile1111	-	-
	H (5-OH)-Cys1070			
	O (5-OH)-Cys1070			
	H (7-OH)-Glu1197			
Hesperidin	H (glycone)-Thr259			
	O (glycone)-Thr259			
	O (glycone)-Thr259			
	H (5-OH)-Glu1080			
	O (glycone)-Arg1184			
	H (glycone)-Ser1113			
	H (glycone)-Ser1113			
	H (glycone)-Glu1115			
H (glycone)-Ile1117				
H (3'-OH)-Asp1196				
Demethylnobiletin	O (7-OCH ₃)-Gln1114	Ring B-Thr259		
	O (8-OCH ₃)-Gln1114	Ring B-Ile1111		
	O (8-OCH ₃)-Glu1115	Ring B-Ile1117	-	-
		Ring B-Ala1181		

Table 3.12 (continued)

Compound	Residue involved in H-bond formation	Residue involved in hydrophobic interaction	Residue involved in aromatic interaction	Residue involved in Charge interaction
5-Hydroxy-3,6,7,8,3',4'-hexamethoxyflavone (5HHMF)	O (4-OH)-Gln1114			
	O (3-OCH ₃)-Gln1114	Ring B-Ile1111	-	-
	H (5-OH)-Glu1115			
	O (4-OH)-Glu1115			
Nobiletin		Ring B-Thr259		
	-	Ring B-Ile1111	-	-
		Ring B-Ile1117		
Positive control				
Verapamil	O (OCH ₃)-Thr806	Benzene ring-Ala255		
	O (OCH ₃)-Thr807	Benzene ring-Ile257	-	-
	N-Glu1115	Benzene ring-Thr259		
		Benzene ring-Ile1117		
Nifedipine	O-Gly1174	Benzene ring-Ala1201	-	-
		Benzene ring-Thr259		
Atorvastatin		F-Thr259		
		Benzene ring-Ala262		
		F-Ala262		
		F-Phe263	-	O (carboxylic group)-Arg258
		Benzene ring1-Ile1111		
		Benzene ring2-Ile1111		
		F-Ile1111		
	Benzene ring-Val1076			
Substrate				
Adenosine triphosphate (ATP)	O-Ser1113			
	O1 (phosphate group)-Gln1114			
	O2 (phosphate group)-Gln1114			
	O (phosphate group)-Glu1115		Adenine ring-Arg1184	-
	H (OH side chain)-Glu1115			
		O (OH side chain)-Ile1117		

Table 3.13 The important amino acid residues of NBD2 that involved in the molecular interactions of P-gp crystal structures (4Q9H) with its inhibitors (flavonoids) identified by LigandScout

Amino acid residue	Number of H-bond involved (Number of compound involved)	Number of hydrophobic interaction involved (Number of compound involved)	Number of aromatic interaction involved (Number of compound involved)	Number of charge interaction involved (Number of compound involved)
Leu254	2 (1)	-	-	-
Ala255 ^a	1 (1)	1 (1)	-	-
Ile257 ^a	-	2 (2)	-	-
Arg258 ^a	7 (6)	-	1 (1)	-
Thr259a	8 (5)	9 (8)	-	-
Ala262a	-	3 (3)	-	-
Phe263 ^a	-	2 (2)	-	-
Phe800	2 (2)	-	-	-
Asp801	1 (1)	-	-	-
Asp802	2 (1)	-	-	-

Table 3.13 (continued)

Amino acid residue	Number of H-bond involved (Number of compound involved)	Number of hydrophobic interaction involved (Number of compound involved)	Number of aromatic interaction involved (Number of compound involved)	Number of charge interaction involved (Number of compound involved)
Thr806 ^a	2 (2)	-	-	-
Thr807 ^a	5 (3)	1 (1)	-	-
Tyr1040	2 (1)	-	-	-
Thr1042	-	1 (1)	-	-
Arg1043	1 (1)	-	-	-
Ser1067	1 (1)	-	-	-
Gly1069	2 (1)	-	-	-
Cys1070	3(2)	-	-	-
Gly1071	1 (1)	-	-	-
Ser1073	1 (1)	-	-	-
Val1076 ^a	2 (2)	1 (1)	-	-
Gln1077	1 (1)	-	-	-
Glu1080	4 (4)	-	-	-
Phe1082	-	2 (2)	-	-
Ile1111 ^a	3 (2)	12 (10)	-	-
Ser1113 ^b	4 (3)	-	-	-
Gln1114 ^b	7 (5)	-	-	-
Glu1115 ^b	13 (9)	-	-	-
Ile1117 ^{a,b}	8 (8)	4 (4)	-	-
Ala1181	-	4 (4)	-	-
Arg1184 ^b	4 (4)	-	-	-
Leu1195	-	1 (1)	-	-
Asp1196	2 (2)	-	-	-
Glu1197	3 (3)	-	-	-
Ala1198	-	3 (3)	-	-
Thr1199	-	3 (3)	-	-
Ser1200	2 (1)	-	-	-
Leu1202	2 (1)	-	-	-
Glu1207	1 (1)	-	-	-
Lys1208	2 (2)	-	-	-
Gln1211	1 (1)	-	-	-
Leu1214	2 (2)	1 (1)	-	-
Arg1218	1 (1)	-	-	-
Val1225	-	3 (3)	-	-
Ala1227	-	3 (3)	-	-
His1228	1 (1)	-	-	-
Arg1229	2 (1)	-	-	-
Thr1232	-	2 (2)	-	-
Ile1233	-	3 (3)	-	-
Asn1235	2 (1)	-	-	-
Ile1242	1 (1)	-	-	-
Asn1244	2 (2)	-	-	-
Ile1046	-	3 (2)	-	-
Val1048	-	2 (2)	-	-

^aAmino acid residues that interact with the positive controls.

^bAmino acid residues that interact with ATP.

In the present, computational-aided drug design and screening of an active compound has emerged as a powerful technique playing a crucial role including structure-based modelling, a method commonly utilised, which has become a useful tool for discovering molecules as an effective hit against particular target. Compounds are usually validated their efficacy in wet lab experiments to produce reliable of data

(Wongrattanakamon et al., 2016). The binding pocket for flavonoids was investigated and found these inhibitors compete with the ATP for binding site (as ATP competitive inhibitors) in NBDs including the NBD amino acid residues of P-gp identified by the *in silico* techniques to be involved in the hydrogen bonding and van der Waals (hydrophobic) interactions with flavonoids (Gadhe et al., 2013) and these reports are likewise consistent the result of this study. Only few flavonoids bind P-gp at different (allosteric) sites. These P-gp allosteric inhibitors may induce a conformational alteration that remodels the shape of the active site and deducts the affinity of the P-gp's active site for ATP. The hotspot amino acid residues that play key roles in the protein-ligand interactions of 25 flavonoids including 3 positive controls within both NBD1 and NBD2 binding sites were clarified that supported the ATP competitive mechanism. Moreover, a residue like Gln1114 is a part of both major and minor binding sites at NBD2 indicating a close relation between both binding sites, and confirming that an allosteric inhibitor binding at NBD2 minor binding site directly affects and blocks ATP to bind the active site. The docking scores of all flavonoid allosteric inhibitors were agreeable with their experimental P-gp inhibitory activities suggesting that a mechanism of action of these compounds still influenced with ATP binding site within both NBDs as allosteric inhibitors and finally prevented ATP to bind with its binding site.

Other previous docking studies of P-gp NBDs also discovered according results. Gadhe et al. (Gadhe et al., 2013) docked a flavonoid; desmosdumotin B into P-gp NBD. Docking study was performed in the homology modelling of NBD2. The desmosdumotin B binding site occupied the ATP binding site (flavonoid binding region) with hydrophobic and hydrophilic interactions. Binding mode analysis results suggest that desmosdumotin B interacts with the NBD2 through both hydrogen bonds and hydrophobic interactions at the same related amino acid residues of our flavonoid-4Q9H NBD2 models which are Tyr1040 (1044), Thr1042 (1046), Arg1043 (1047), Val1048 (1052), Ser1067 (1071), Gly1069 (1073), Cys1070 (1074), Gly1071 (1075), Ser1073 (1077), and Gln1077 (1081). The obtained results support the mechanism of P-gp inhibition of flavonoids that compete with the ATP for binding site as ATP competitive inhibitors.

Furthermore, the study regarding non-flavonoid compounds also provided the same inhibition patterns of P-gp. Brewer et al. (Brewer et al., 2014) described

exceedingly high-throughput, massively parallel *in silico* ligand docking studies had an intention of analysing reversible inhibitors of ATP hydrolysis that target the NBDs of this protein. They utilised a structural human P-gp model as the protein target for ligand docking to identify ligands that bound prominently to the NBDs. Four docked non-flavonoid compounds were found to be inside ATP-binding pockets of NBD1 and NBD2. The amino acid residues of the pockets within 5.0 Å of the docked inhibitors possibly interacting to four ligands and relating to our NBD1 and NBD2 model residues which were Asp160 (164), Tyr397 (401), Ser430 (434), Gln434 (438), Leu439 (443), Gln471 (475), Val520 (524), Gly521 (525), Glu522 (526), Ala525 (529), Leu527 (531), and Arg901 (905) at NBD1; and Arg258 (262), Phe800 (804), Asp801 (805), Tyr1040 (1044), Arg1043 (1047), Val1048 (1052), Ser1073 (1077), Gln1077 (1081), Gln1114 (1118), and Gly1174 (1178) at NBD2. Our docking result found that most ligands (flavonoids, ATP and control drug inhibitors) interacted to these residues inside the major binding pockets of both NBDs. The experimental result likewise confirmed that these non-flavonoid compounds inhibited ATP hydrolysis by P-gp in the *in vitro* test.

Saeed et al., (Saeed et al., 2015) generated the homology model of human P-gp utilised for molecular docking of one flavonoid compound; apigenin. Their result showed that this flavonoid bound to the highly conserved NBD1 pointing out that apigenin meddles with ATP binding and cleavage. Rather than to drug pharmacophores in the P-gp transmembrane domain, flavonoids bind to the ATP binding sites of the protein. Their data point out that apigenin may bind to the ATP binding sites of P-gp and consequently competes with ATP for binding. Therefore, ATP cannot be hydrolysed and the energy is not available to fuel the P-gp substrates transport. Apigenin bound to the ATP binding site of NBD1 (the major binding site of our study) and the corresponding hot spot residue; Tyr 401 (Tyr397 of 4Q9H) involving in the interaction was shown. Moreover, Zeino et al. (Zeino et al., 2014) clarified that Gln1118 (Gln1114 of 4Q9H) was the key amino acid residue inside the major binding pocket of NBD2 responsible for the interaction with apigenin and our result illustrated that this residue was very important for P-gp to interact with ATP.

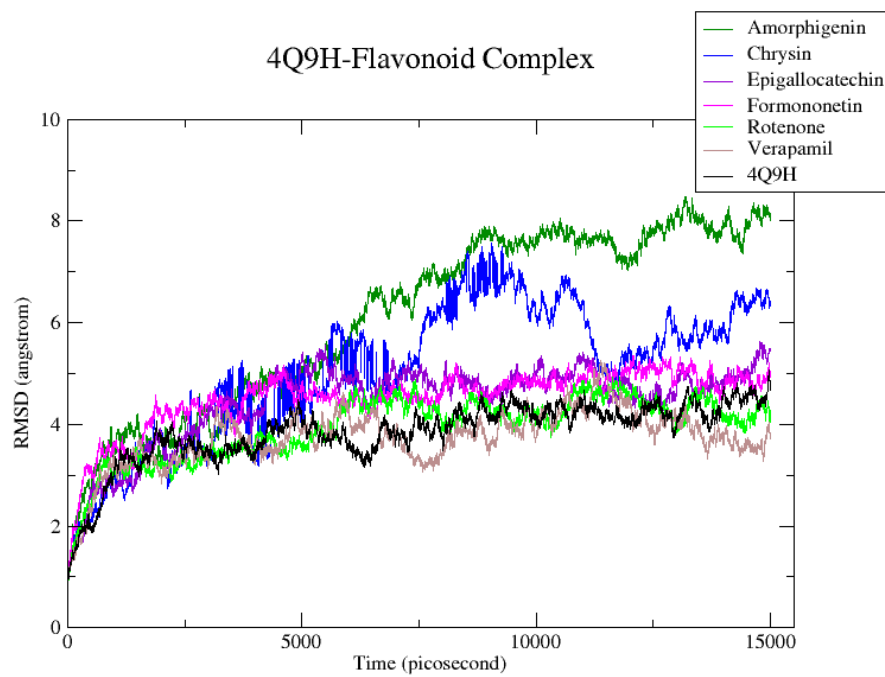
3.3 Molecular dynamics (MD) simulations of P-gp inhibitors

3.3.1 Trajectory analysis

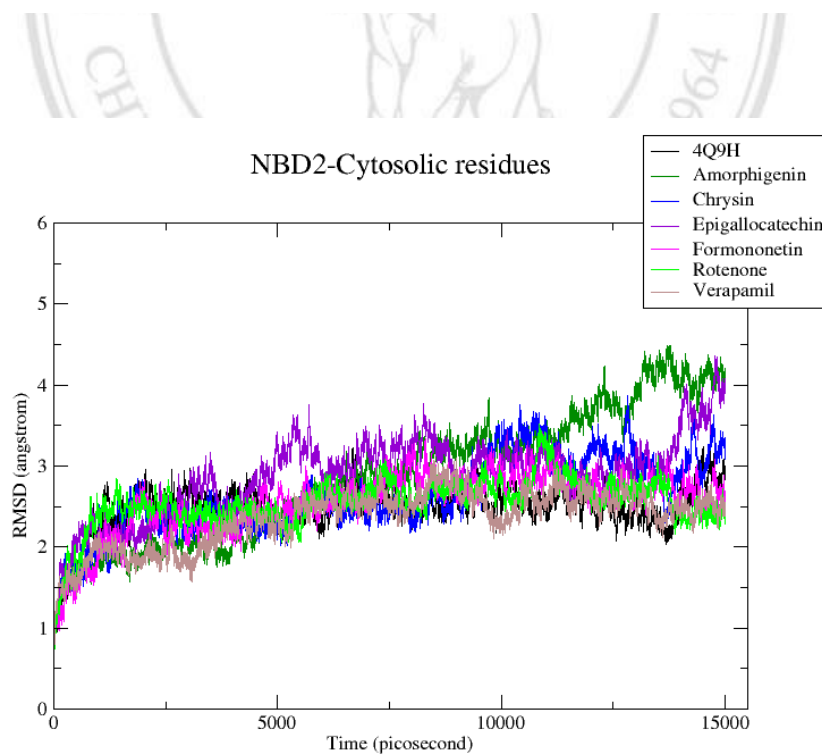
Each selected docking conformation of 4Q9H–flavonoid complex generated by Autodock was taken as an initial conformation for MD simulation for intimate binding interaction analysis in dynamic state. To determine an average deviation in the atomic positions/stability of MD trajectory, the atomic RMSD of protein backbone of each trajectory was drawn versus time (Figure 3.6) with respect to its initial structure. Every trajectory posterior 10000 ps of the production run was found to be quite stable with small deviations within a range of 3 Å (Lazaridis & Karplus, 1999) compared to apo 4Q9H in the conformation of backbone of the protein (Figure 3.6a). Thus, we can strongly confirm these compounds to be potent inhibitors of P-gp. Furthermore, the RMSD plots of flavonoid binding (cytosolic) residues (Figure 3.6b) and ligands (Figure 3.6c) illustrated that all MD trajectories were steady to be further operated a binding energy measurement and molecular binding interaction identification.

The cytosolic residues of all complexes maintained stable showing deviation within 1 Å compared to apo 4Q9H (Figure 3b), indicating the favourable binding interactions occurring in the NBD2. The conformational alterations related with every flavonoid in the NBD2 and their atomic deviations in the NBD2 were analysed. Figure 3c illustrates RMSD versus time plots of all flavonoids. All of the flavonoids kept stable interactions within the NBD2 illustrating deviation within 2 Å with respect to its initial position, indicating their favourable binding in the NBD2. In the case of rotenone, a relative shift in atomic position was observed posterior 8000 ps. On visual examination of each MD trajectory it was remarked that rotenone was slightly moved from the site with respect to its initial position. Verapamil (positive control) showed the noticeable highest deviation within 2.5 Å which was consistent all over the trajectory, wherewith higher flexibility in the molecular structure than the flavonoids (Prajapati et al., 2013).

a.



b.



C.

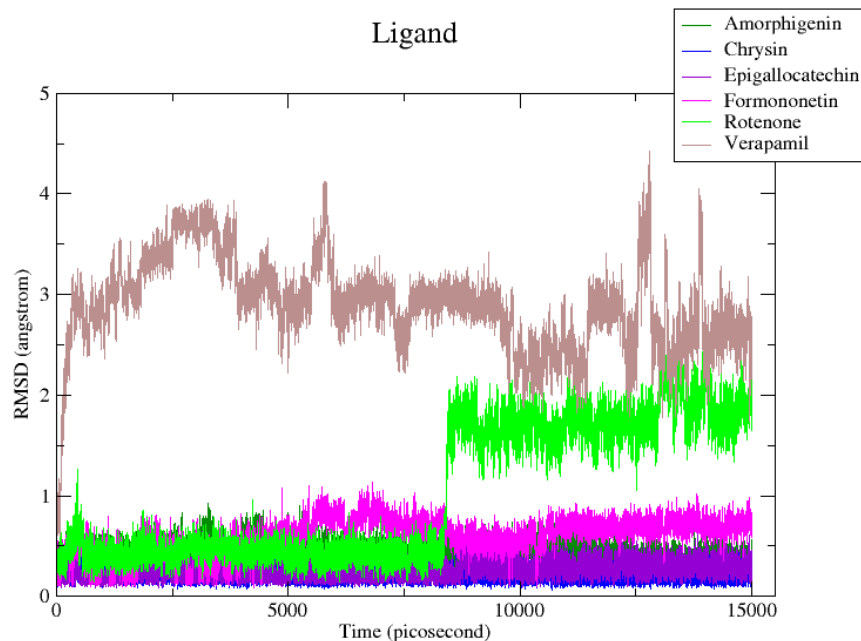


Figure 3.6 Plot of root mean square deviations (RMSD) versus time (ps) obtained over a time course of 15000 ps production for (a) the backbone atom (C_{α} , N, C) of the protein–ligand complexes, (b) NBD2-Cytosolic residues, and (c) ligands

3.3.2 Pre and post MD simulation binding mode analysis

Binding modes of the flavonoids were analysed in NBD2 active site and presented in Figure 3.7-3.12. The binding site for flavonoids was defined with the prior knowledge of active site residues as well as by keeping in mind that these compounds compete with the ATP for binding site (Gadhe, Kothandan, & Cho, 2013). Furthermore, the docking result revealed that all flavonoids occupied the same site of ATP. ATP interacted with Ser1113, Gln1114, Glu1115, Ile1117 residues.

Average binding modes of every compound were calculated and analysed from average structures of the complexes throughout the stable stage (last 10000 to 15000 ps of simulations) that there were no significant alterations in the stability of the complexes. Important molecular interactions such as hydrogen bonds, hydrophobic interactions, and so forth were studied by interaction network visualising using LigandScout. After MD simulation (in the stable stage), position of each flavonoid was somehow shifted when compared with the original docked mode in binding pocket of

NBD2, and well positioned into the NBD2 active site with hydrogen bonds and hydrophobic interactions. Hydrogen bond distance measurement was based on the distance between heavy atoms which is incorporated in generation of hydrogen bond in such way that the distance is not over 3.5 Å (Mirzaie et al., 2013).

The initial binding of amorphenin (identified in the docking study), the oxygen atoms at 12-position and hydroxyl side chain of ring E formed two hydrogen bonds with Arg258 and Arg1184 of 4Q9H respectively (Figure 3.7a), two of the active site residues in NBD2. Five hydrophobic bonds between alkene side chain of ring E–Thr259, ring D–Ala262, alkene side chain of ring E–Ile1111, ring D–Ile1111, and alkene side chain of ring E–Ala1181 (Figure 3.7a) were also identified. In the stable stage, a slightly different interaction pattern was observed. The structure-based models clearly show the relative shift of amorphenin from the initial binding site. Amorphenin was now involved in hydrophobic interactions between ring D–Ile1117, alkene side chain of ring E–Phe1119, ring D–Phe1119, alkene side chain of ring E–Tyr1129, and ring D–Tyr1129 and aromatic (pi stacking) interaction between ring D–Tyr1129 (Figure 3.7b). Amorphenin was forming two new hydrogen bonds with Thr259 and Cys1121 throughout the stable stage (Figure 3.7b). The distances represent hydrogen bonds between O6-atom of amorphenin–O-atom of active site residue Thr259 and O7-atom of amorphenin–S-atom of active site residue Cys1121 were plotted (Figure 3.7c). The formation of two hydrogen bonds including five hydrophobic and one pi stacking interactions contributed to a higher stability between amorphenin and 4Q9H. Stable in hydrogen bond distances were observed towards the stable stage simulation period, suggesting strong of the hydrogen bonds at these amino acid residues. Amorphenin is classified as rotenoids. It was noted that the ring D and alkene group on ring E, and O-atoms of methoxy and hydroxyl groups of amorphenin are very important for molecular interactions (pi stacking/hydrophobic interactions and hydrogen bond respectively) with amino acid residues to hold the ligand tightly into the binding cavity during MD simulation including O atom at 12-position that is also essential for initial hydrogen bond interaction.

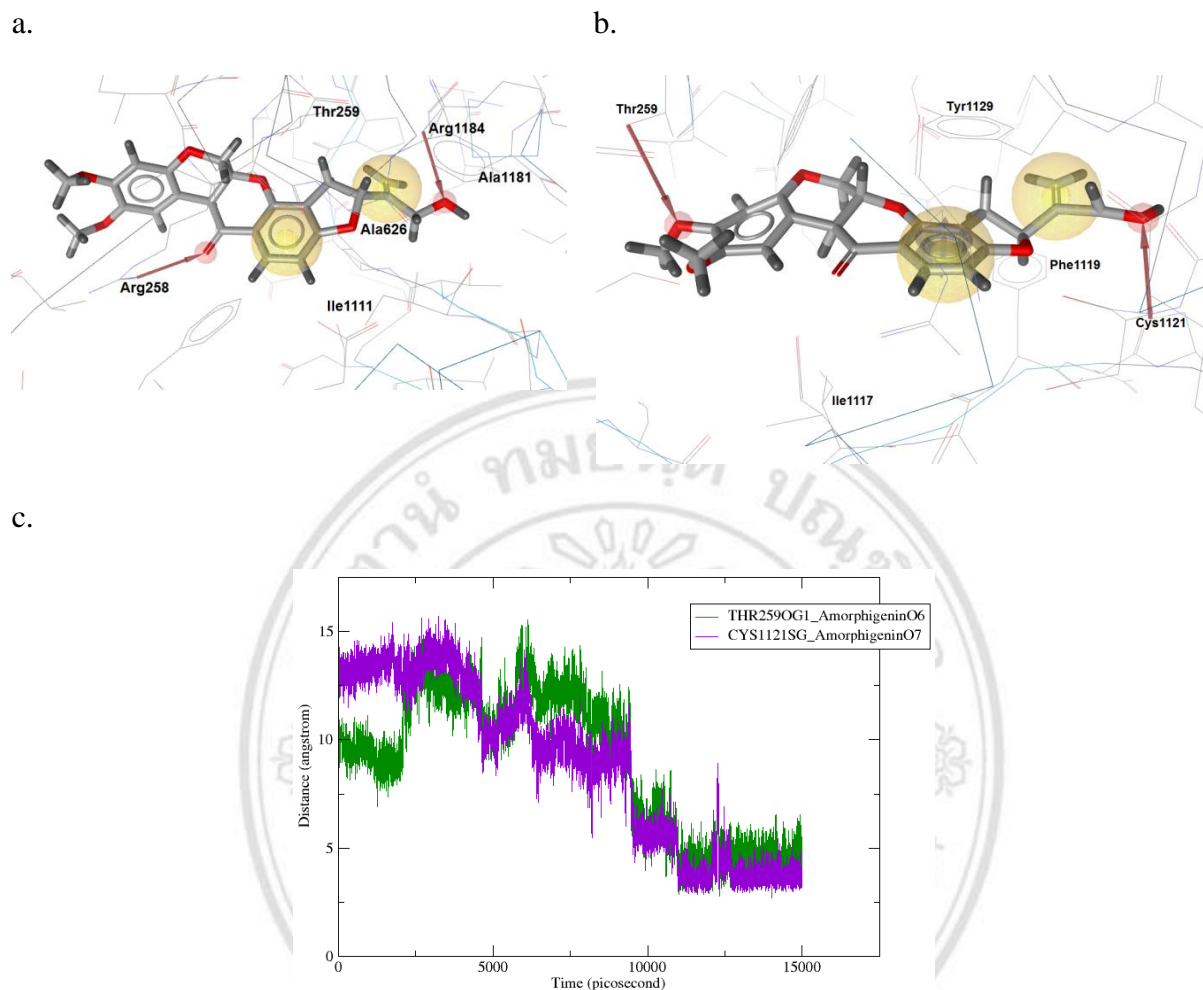


Figure 3.7 Structure-based pharmacophore models illustrate molecular interactions of 4Q9H–amorphigenin. (a) pre-MD interactions, (b) post-MD interactions of the average structure throughout the stable stage (10000-15000 ps), and (c) new formed hydrogen bond distances between 4Q9H–amorphigenin throughout the stable stage

The initial binding of chrysin, the oxygen of hydroxyl side chain at 7-position formed one hydrogen bond with Gln1114 and two hydrogen bonds with Ser1200 of 4Q9H (Figure 3.8a), two of the active site residues in NBD2. Five hydrophobic bonds between ring B– Ala1198, Thr1199, Val1225, Ala1227, and Ile1233 (Figure 3.8a) were also identified. In the stable stage, a little different interaction pattern was observed. The structure-based models clearly show the slight relative shift of chrysin from the initial binding site, however, this change did not affect the stability of the complex. Docking identified hydrophobic interactions between ring B of chrysin and Ala1198, Thr1199, Ala1227 were maintained during MD simulation but Val1225, Ile1233 were changed

after MD simulation, and three new amino acid residues (Leu1195, Leu1214, and Thr1232) were introduced in the vicinity of chrysin (Figure 3.8b). Chrysin was forming new hydrogen bond with His1228 throughout the stable stage (Figure 3.8b). The distance represents a hydrogen bond between O3-atom of chrysin–N-atom of active site residue His1228 was plotted (Figure 3.8c). The formation of one hydrogen bond including six hydrophobic interactions contributed to a high stability between chrysin and 4Q9H. Stable in hydrogen bond distance was observed at 1000 ps towards the stable stage simulation period, suggesting strong of the hydrogen bond at this amino acid residue. Chrysin is classified as flavones. It was noted that the ring A has two surrounding hydrophilic hydroxyl groups, therefore leading to ring A more tough to allow a hydrophobic interaction in the binding cavity. So the ring B and including O atom at 4-position of chrysin are very essential to provide hydrophobic interactions and hydrogen bond respectively with amino acid residues to hold the ligand tightly into the binding cavity during MD simulation as well as the oxygen of 7-hydroxyl group that is also essential for initial hydrogen bond interaction.

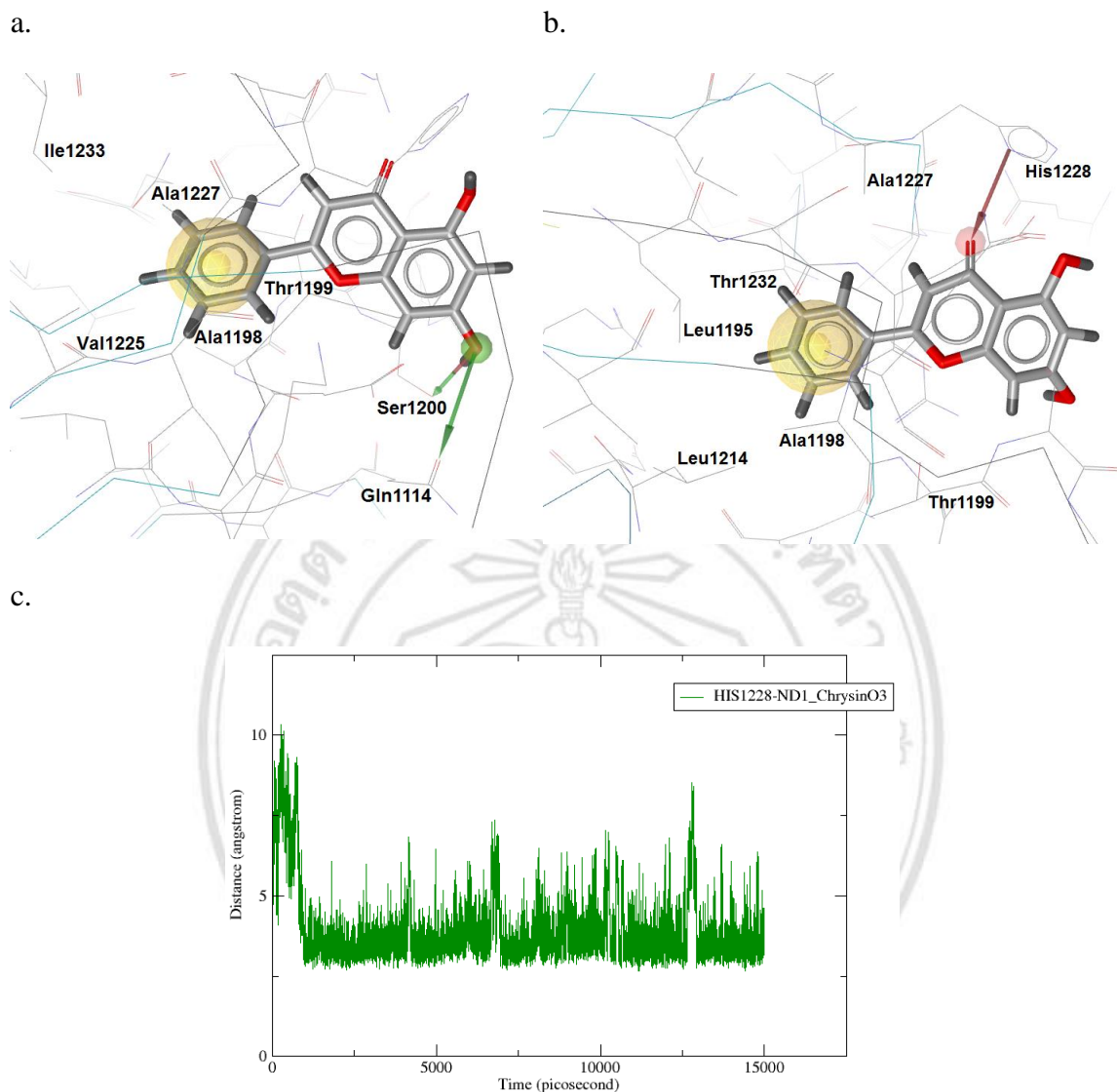


Figure 3.8 Structure-based pharmacophore models illustrate molecular interactions of 4Q9H–chrysin. (a) pre-MD interactions, (b) post-MD interactions of the average structure throughout the stable stage (10000-15000 ps), and (c) a new formed hydrogen bond distance between 4Q9H–chrysin throughout the stable stage

Epigallocatechin is one of catechins characterised by multiple of hydroxyl groups; hydrophilic side chains on the rings (Velayutham, Babu, & Liu, 2008) (Figure 3.9). The initial binding of epigallocatechin, the oxygen atoms of several hydroxyl side chains including at 7-position formed one hydrogen bond with Glu1080, 3'-position formed one hydrogen bond with Gln1114, 4' and 5'-positions formed each one hydrogen bond with Glu1115, and 3-position formed two hydrogen bonds with Glu1115, and Ile1117 of 4Q9H (Figure 3.9a). No hydrophobic bond was identified. In the stable stage, a

different interaction pattern was observed. The structure-based models clearly show more relative shift of epigallocatechin from the initial binding site compared to amorphenin and chrysin, however, this change slightly affected the stability of the complex. Docking identified hydrogen bonds between epigallocatechin and amino acid residues were changed after MD simulation, and two new amino acid residues (Thr259 and Thr1042) were introduced in the vicinity of epigallocatechin (Figure 3.9b). The oxygen atoms of hydroxyl groups at 4' and 7-positions of epigallocatechin were forming new hydrogen bonds with these binding site residues respectively throughout the stable stage (Figure 3.9b). The distances represent between O6-atom of epigallocatechin–O-atom of active site residue Thr259 and O7-atom of epigallocatechin–O-atom of active site residue Thr1042 were plotted (Figure 3.9c). The formation of both hydrogen bonds contributed to a high stability between epigallocatechin and 4Q9H. Stables in both hydrogen bond distances were observed at 8750 ps towards the stable stage simulation period, suggesting strong of the hydrogen bonds at these amino acid residues. Epigallocatechin is classified as flavan-3-ols. It was noted that epigallocatechin possesses single bonds that prevents electron delocalisation over the ring C (Fraga, Celep, & Galleano, 2009) and many surrounding polar hydroxyl groups, thus rendering it more difficult to provide pi stacking/hydrophobic interactions in the binding pocket (Phan et al., 2014), however, the multiple of hydroxyl groups is very important and beneficial in generating strong hydrogen bond interactions with amino acid residues to hold the ligand tightly into the binding cavity during MD simulation including also essential for initial binding interaction.

ลิขสิทธิ์มหาวิทยาลัยเชียงใหม่
Copyright © by Chiang Mai University
All rights reserved

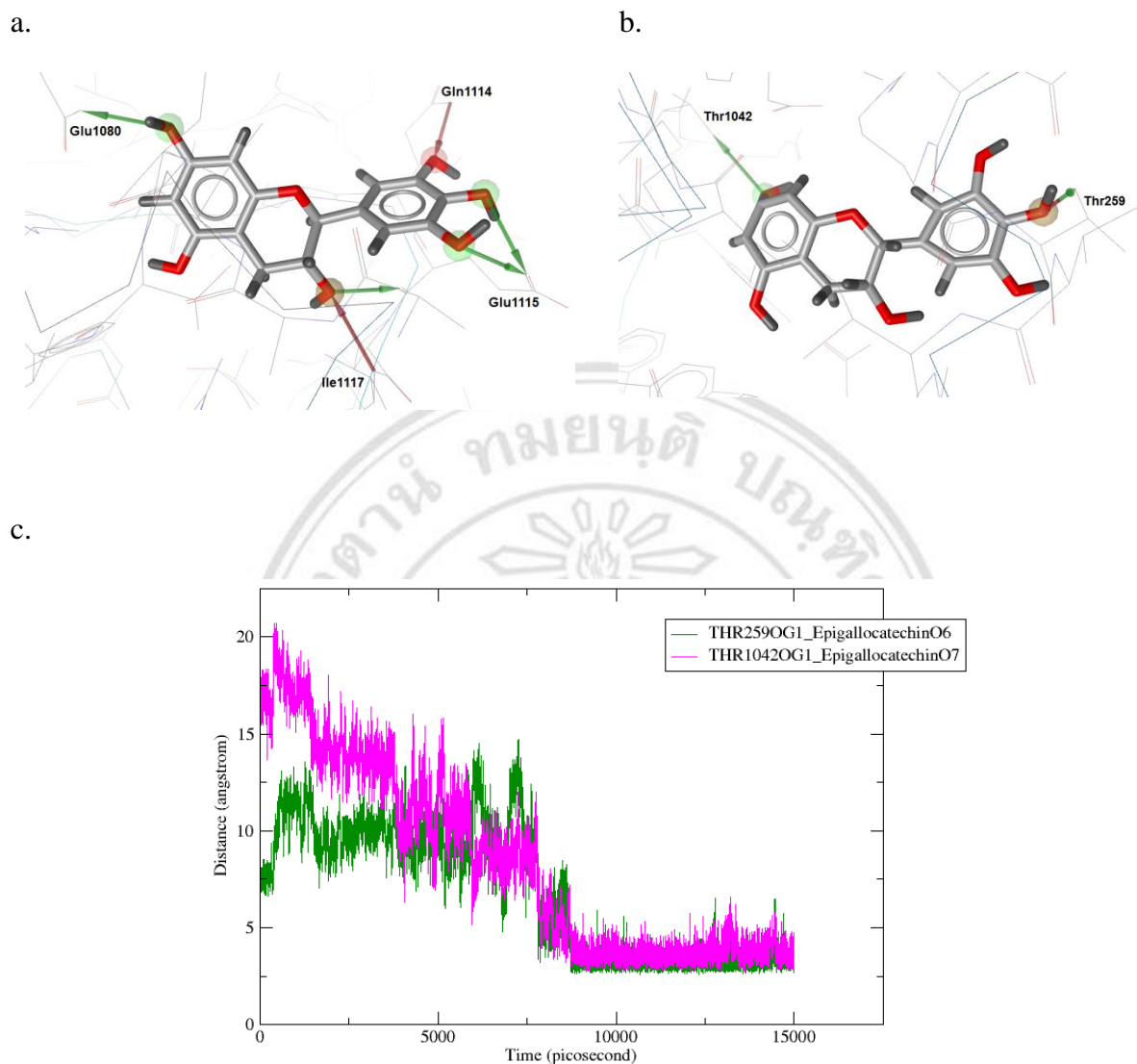


Figure 3.9 Structure-based pharmacophore models illustrate molecular interactions of 4Q9H-epigallocatechin. (a) pre-MD interactions, (b) post-MD interactions of the average structure throughout the stable stage (10000-15000 ps), and (c) new formed hydrogen bond distances between 4Q9H- epigallocatechin throughout the stable stage

The initial binding of formononetin, the oxygen of hydroxyl side chain at 7-position formed one hydrogen bond with Glu1197 (Figure 3.10a), one of the active site residue in NBD2. Seven hydrophobic bonds between ring B–Leu1195, ring B–Ala1198, ring A–Thr1199, ring B–Leu1214, ring B–Val1225, ring A–Ala1227, and ring B–Ile1233 (Figure 3.10a) were also identified. In the stable stage, a little different interaction pattern was observed. The structure-based models clearly show the slight relative shift of formononetin from the initial binding site, however, this change

did not affect the stability of the complex. Docking identified hydrophobic interactions between ring B–Leu1214 and ring A–Ala1227 were maintained during MD simulation but Leu1195, Ala1198, and Val1225 switched to interact with ring A after MD simulation, and one new amino acid residue (Thr1232) interacting with ring A was introduced in the vicinity of formononetin (Figure 3.10b). The only one occurring hydrogen bond between formononetin and NBD2 was moved to the adjacent residue; ALA1198 throughout the stable stage (Figure 3.10b). The distance represents a hydrogen bond between O4-atom of formononetin–N-atom of active site residue Ala1198 was plotted (Figure 3.10c). The formation of one hydrogen bond including six hydrophobic interactions contributed to a high stability between formononetin and 4Q9H. Stable in hydrogen bond distance was observed at 11000 ps towards the stable stage simulation period, suggesting strong of the hydrogen bond at this amino acid residue. Formononetin is classified as isoflavones. It was noted that the ring A and B of formononetin, and the oxygen of 7-hydroxyl group are very important for hydrophobic interactions and hydrogen bond respectively with amino acid residues to hold the ligand tightly into the binding cavity at initial binding and during MD simulation.

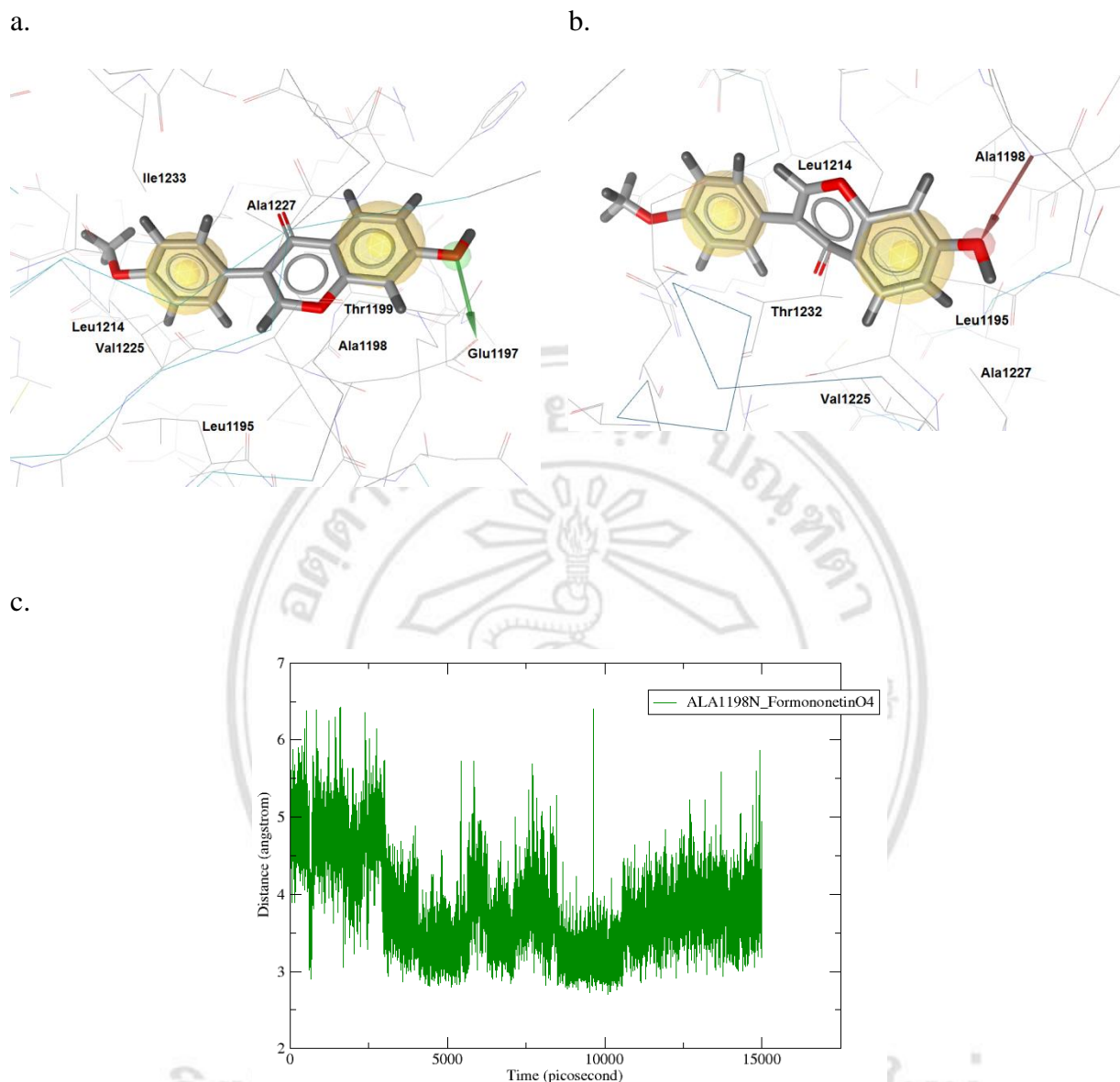


Figure 3.10 Structure-based pharmacophore models illustrate molecular interactions of 4Q9H-formononetin. (a) pre-MD interactions, (b) post-MD interactions of the average structure throughout the stable stage (10000-15000 ps), and (c) a new formed hydrogen bond distance between 4Q9H-formononetin throughout the stable stage

The initial binding of rotenone, the oxygen atoms at 12-position formed one hydrogen bond with Arg258 of 4Q9H respectively (Figure 3.11a), one of important active site residues in NBD2. Five hydrophobic bonds between alkene side chain of ring E-Thr259, ring D-Thr259, alkene side chain of ring E-Ile1111, ring D-Ile1111, and alkene side chain of ring E-Ala1181 (Figure 3.11a) were also identified. In the stable stage, a little different interaction pattern was observed. The structure-based models

clearly show the slight relative shift of rotenone from the initial binding site. Docking identified all hydrophobic interactions were maintained during MD simulation, and two new amino acid residue (Phe263, Ile1117) hydrophobic interacting with alkene group were introduced in the vicinity of rotenone (Figure 3.11b). Rotenone was not forming any new hydrogen bonds with active residues throughout the stable stage (Figure 3.11b). The formation of seven hydrophobic interactions contributed to a high stability between rotenone and 4Q9H. Rotenone is classified as rotenoids. It was noted that the ring D, and alkene group on ring E of rotenone are very important for molecular hydrophobic interactions with amino acid residues to hold the ligand tightly into the binding cavity during MD simulation including O atom at 12-position that is also essential for initial hydrogen bond interaction.

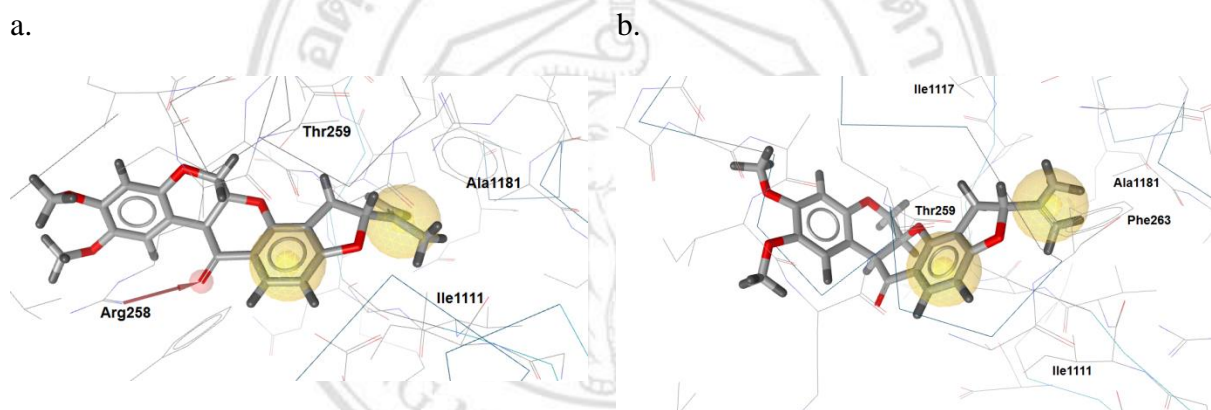


Figure 3.11 Structure-based pharmacophore models illustrate molecular interactions of 4Q9H-rotenone. (a) pre-MD interactions, (b) post-MD interactions of the average structure throughout the stable stage (10000-15000 ps), no hydrogen bonds is formed throughout the stable stage

Towards the initial binding of verapamil, two oxygen atoms of the methoxy groups formed three hydrogen bonds with Thr806 and Thr807, and N atom of the nitrile group formed one hydrogen bond with Glu1115 of 4Q9H (Figure 3.12a). These are the important active site residues in NBD2. Five hydrophobic bonds between the benzene ring-Ala255, benzene ring-Ile257, benzene ring-Thr259, benzene ring-Thr807, and benzene ring-Ile1117 (Figure 3.12a) were also identified. In the stable stage, a little different interaction pattern was observed. The structure-based models clearly show the slight relative shift of verapamil from the initial binding site. Docking identified hydrophobic interactions between benzene ring-Ala255, benzene ring-Thr259, and

benzene ring–Ile1117 were maintained during MD simulation and one new amino acid residue (Ala256) interacting with benzene ring was introduced in the vicinity of verapamil (Figure 3.12b). Verapamil was not forming any new hydrogen bonds with active residues throughout the stable stage (Figure 3.12b). The formation of five hydrophobic interactions contributed to a high stability between verapamil and 4Q9H. Verapamil has been discoursed as a P-gp substrate. It is known as a strong inhibitor of P-gp function and used like a positive control inhibitor of P-gp. The structure of verapamil is great molecular flexibility (Nonnenmacher, Brouant, Mrozek, Karolak-Wojciechowska, & Barbe, 2000). It was noted that two benzene rings, and alkane group of verapamil are very important for molecular hydrophobic interactions with amino acid residues to hold the ligand tightly into the binding cavity during MD simulation including O atoms of methoxy side chains that is also essential for initial hydrogen bond interaction.

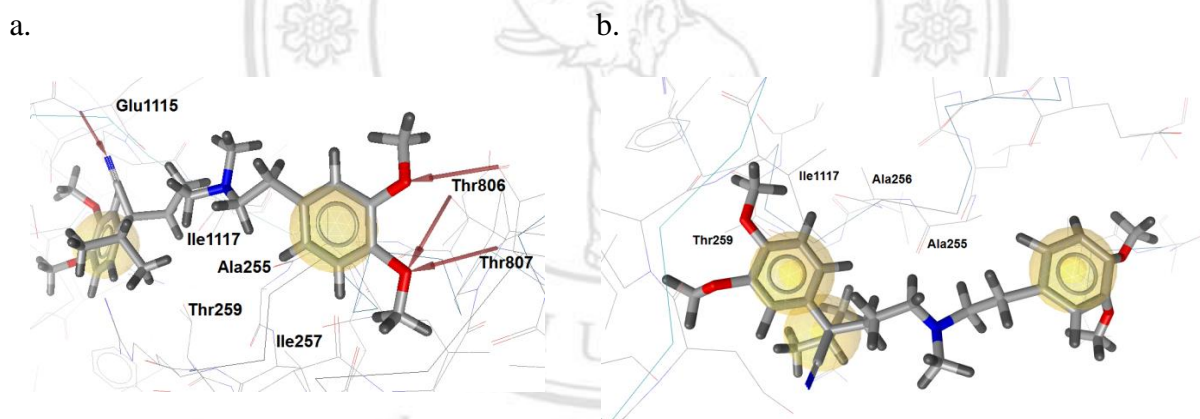


Figure 3.12 Structure-based pharmacophore models illustrate molecular interactions of 4Q9H–verapamil. (a) pre-MD interactions, (b) post-MD interactions of the average structure throughout the stable stage (10000–15000 ps), no hydrogen bonds is formed throughout the stable stage

3.3.3 Binding free energy calculation

The binding free energies (PB_{TOT}) and contribution energies between 4Q9H and flavonoids were summarised in Table 3.14. More negative values pointed out more favourable binding. The calculations from MM-PBSA over 15000 ps were better agreed with the experimental data than MM-GBSA method. Thus, each simulation was compared to one and another utilising the PB_{TOT} value. The binding free energies of

amorphigenin, chrysin, epigallocatechin, formononetin, and rotenone to 4Q9H were -25.07, -26.28, -16.93, -30.68, and -14.29 kcal/mol respectively that were approximate to -20.62 kcal/mol of the positive control verapamil, indicating that these flavonoids bound tightly to 4Q9H as though did verapamil.

Table 3.14 Contribution of energies to binding free energy of 4Q9H–flavonoid complex

Method	Contribution	Energy in each contribution (kcal/mol)					
		Amorphigenin	Chrysin	Epigallocatechin	Formononetin	Rotenone	Verapamil
MM	ELE	-9.86	0.32	-0.09	0.50	-5.46	3.77
	VDW	-45.40	-41.13	-30.03	-46.68	-37.59	-43.75
	INT	5.87	-0.00	0.00	-0.00	-0.00	0.00
	GAS	-49.39	-40.82	-30.12	-46.18	-43.06	-39.98
PBSA	PB _{SUR}	-5.11	-3.75	-3.56	-4.33	-5.54	-6.58
	PB _{CAL}	29.43	18.28	16.75	19.83	34.31	25.93
	PB _{SOL}	24.32	14.53	13.19	15.50	28.77	19.36
	PB _{ELE}	19.57	18.60	16.66	20.33	28.84	29.70
	PB _{TOT}	-25.07	-26.28	-16.93	-30.68	-14.29	-20.62
GBSA	GB _{SUR}	-3.55	-2.61	-2.47	-3.01	-3.85	-4.57
	GB	21.01	13.35	13.78	13.53	25.98	16.54
	GB _{SOL}	17.46	10.75	11.30	10.52	22.13	11.97
	GB _{ELE}	11.15	13.67	13.68	14.03	20.52	20.31
	GB _{TOT}	-31.93	-30.07	-18.82	-35.66	-20.92	-28.01

Note: ELE: non-bonded electrostatic energy, VDW: non-bonded van der Waals energy, INT: internal energies (bond, angle, dihedral energies), GAS: MM energies = ELE+VDW+INT, PB_{SUR}: non-polar contribution to solvation, PB_{CAL}: polar contribution of solvation, PB_{SOL}= PB_{SUR}+PB_{CAL}, PB_{ELE}= PB_{CAL}+ELE, PB_{TOT}: total binding free energy calculated by the MM-PBSA method = PB_{SOL}+GAS, GB_{SUR}: non-polar contribution to solvation, GB: polar contribution of solvation, GB_{SOL}= GB_{SUR}+GB, GB_{ELE}= GB+ELE, GB_{TOT}: total binding free energy calculated by the MM-GBSA method = GB_{SOL}+GAS

3.3.4 Residue-based energy decomposition

In order to delineate into the mechanism of protein–ligand interactions and to identify the contributions of the key amino acid residues related with binding interactions, the free energy of binding of each P-gp–flavonoid complex was decomposed on key residues in the binding cavity using the MM-GBSA method. Therefore, decomposed energies on a pairwise per-residue basis were measured. Figure 3.13 illustrates the energy decomposition values for hot-spot amino acid residues in the

complexes. Ordinarily, if the molecular interaction energy between an amino acid residue and ligand is lower than -0.8 kcal/mol, the residue is considered to be a significant amino acid residue in the molecular recognition of that ligand for stabilisation within a binding cavity (Fang et al., 2014).

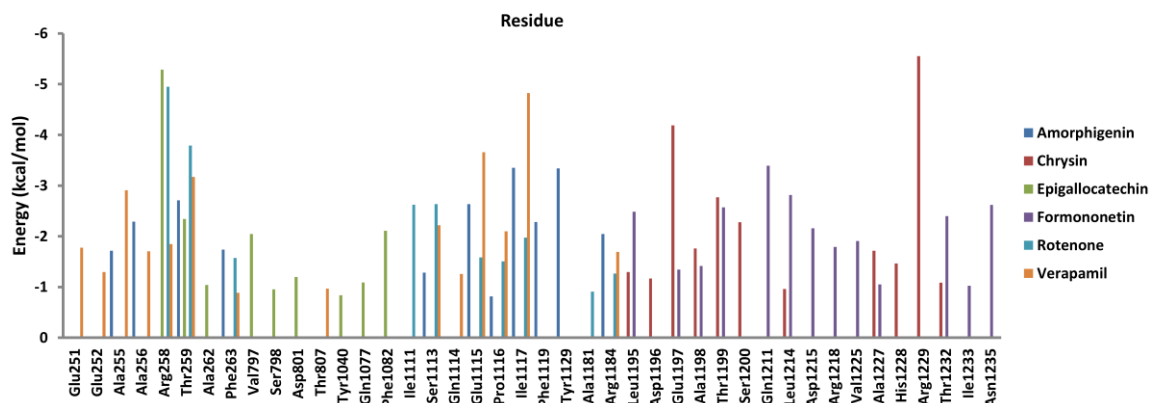


Figure 3.13 Relative decomposed free energies during 15000 ps of important amino acid residues of 4Q9H NBD2 interacting with all flavonoids and verapamil

From Figure 3.13, regarding the complex of 4Q9H–amorphigenin, the main favourable energy contributions (-3.35 to -0.82 kcal/mol) evoke prominently by Ala255 (-1.71), Ala256 (-2.29), Thr259 (-2.71), Phe263 (-1.74), Ser1113 (-1.29), Glu1115 (-2.64), Pro1116 (-0.82), Ile1117 (-3.35), Phe1119 (-2.28), Tyr1129 (-3.34), Arg1184 (-2.05). Regarding the complex of 4Q9H–chrysin, the main favourable energy contributions (-5.55 to -0.96 kcal/mol) evoke prominently by Leu1195 (-1.30), Asp1196 (-1.17), Glu1197 (-4.19), Ala1198 (-1.76), Thr1199 (-2.77), Ser1200 (-2.28), Leu1214 (-0.96), Ala1227 (-1.71), His1228 (-1.47), Arg1229 (-5.55), and Thr1232 (-1.09). Regarding the complex of 4Q9H–epigallocatechin, the main favourable energy contributions (-5.29 to -0.95 kcal/mol) evoke prominently by Arg258 (-5.29), Thr259 (-2.34), Ala262 (-1.04), Val797 (-2.04), Ser798 (-0.95), Asp801 (-1.20), Tyr1040 (-0.84), Gln1077 (-1.09), and Phe1082 (-2.11). Regarding the complex of 4Q9H–formononetin, the main favourable energy contributions (-3.39 to -1.03 kcal/mol) evoke prominently by Leu1195 (-2.48), Glu1197 (-1.34), Ala1198 (-1.41), Thr1199 (-2.57), Gln1211 (-3.39), Leu1214 (-2.82), Asp1215 (-2.16), Arg1218 (-1.79), Val1225 (-1.91), Ala1227 (-1.05), Thr1232 (-2.40), Ile1233 (-1.03), and Asn1235 (-2.62). Regarding the 4Q9H–rotenone complex, the main favourable energy contributions (-4.95 to -0.91 kcal/mol) evoke prominently by Arg258 (-4.95), Thr259

(-3.79), Phe263 (-1.57), Ile1111 (-2.63), Ser1113 (-2.63), Glu1115 (-1.58), Pro1116 (-1.50), Ile1117 (-1.97), Ala1181 (-0.91), and Arg1184 (-1.26). Regarding the complex of 4Q9H-verapamil, the main favourable energy contributions (-4.82 to -0.89 kcal/mol) evoke prominently by Glu251 (-1.78), Glu252 (-1.30), Ala255 (-2.91), Ala256 (-1.70), Arg258 (-1.85), Thr259 (-3.17), Phe263 (-0.89), Thr807 (-0.97), Ser1113 (-2.22), Gln1114 (-1.26), Glu1115 (-3.66), Pro1116 (-2.10), Ile1117 (-4.82), and Arg1184 (-1.69).

Some previous studies clarified that a significant number of enzyme activities are restrained by polyphenols such as flavonoids. For interactions between polyphenol and protein, general chemical characteristics are mostly associated to: (1) a hydrophobicity of aromatic nuclei of each polyphenolic compound, (2) an availability of multiple phenolic hydroxyl groups that provide hydrogen bonding interactions, and (3) a conceivable conjugated π -system between the AC or B ring systems and amino acid residues. On the other hand, flavonoid ligands (flavonols, flavanones, and isoflavones) without any protein inhibitory activities do not form the as stated interactions with active site residues (Fraga et al., 2009). Hydroxyl groups at C7-position of flavonoids: chrysin (flavones), epigallocatechin (flavan-3-ols), and formononetin (isoflavones) are important for hydrogen bond formation with hot spot amino acid residues. Hydrophobicity of ring A and B of chrysin and formononetin are important factors for generating a hydrophobic interaction within ATP binding site of NBD2. For rotenoids (amorphigenin, and rotenone), ring D and alkene group, and oxygen at C12-position are important for hydrophobic interaction and hydrogen bond formations respectively between molecules of rotenoids and the binding pocket. These networks of strong hydrogen and hydrophobic bonds were stable holding the flavonoids in the binding pocket at ATP binding site of NBD2.

The aforementioned studies of Gadhe et al. (Gadhe et al., 2013) showed that the important residues contributing for initial binding of desmosdumotin B to NBD2 was Tyr1044 (1040 of mouse P-gp) which formed the pi stacking interaction with ring B was maintained during MD simulation that pointed out importance of this amino acid residue to grab the ligand solidly into the NBD2 cavity. Thr1046 (1042 of mouse P-gp) residue were also identified to produce hydrophobic interaction with ring B of desmosdumotin B during simulation. These important residues conformed to our

identified residues that Tyr1040 and Thr1042 contributed hydrophobic interaction and hydrogen bond formation respectively with epigallocatechin throughout MD simulation. Moreover, the aforementioned studies of Zeino et al. (Zeino et al., 2014) clarified that Gln1118 (1114 of mouse P-gp) was the important amino acid residue inside the major binding pocket of NBD2 responsible for the interaction with apigenin and also involved in the interaction with ATP. This important residue corresponded to our identified residue that Gln1114 formed hydrogen bond with chrysin and epigallocatechin in the initial interactions and contributed verapamil to firmly bind to NBD2 throughout MD simulation. The previous *in vitro* experiment has confirmed some flavonoids that bind to the NBD and result in blocking drug transport likely by inhibiting P-gp ATPase activity. NBD2 intrinsic fluorescence was also highly quenched upon interaction with flavonoids (Di Pietro et al., 1999). Various flavonoids (apigenin, genistein, kaempferide, naringenin, quercetin, and rutin) bound directly to the expressed purified NBD2 of P-gp, as shown by quenching of the intrinsic Trp fluorescence. Occupancy of the flavonoid binding site by kaempferide blocked ATP binding, indicating that the flavonoid and ATP binding sites overlap (Sharom et al., 1999).

Regarding all complexes, the main favourable energy contributions produced from hydrophobic residues [Ala, Phe, Val, Tyr, Ile, Pro, and Leu (Armstrong et al., 1998)] and Polar, hydrophilic, or charge residues [Arg, Thr, His, Asn, Ser, Asp, Gln, Glu (Petrescu et al., 2004)] within the binding cavity at NBD2. In addition to Ala, Phe, Val, Tyr, Ile, Pro, and Leu that contributed hydrophobic interactions, they also provided contributions to electrostatic interactions or hydrogen bonds that may be due to their hydrophilic groups such as carbonyl group, and so forth (Agarwal et al., 2002; Chou et al., 2003; Palczewski et al., 2000; Takahashi et al., 1989; Williams et al., 2003). Polar, hydrophilic, or charge amino acids, apart from contributing electrostatic interactions, like Arg, Thr, His, Asn, and Gln they also provided contributions to hydrophobic interactions that may be on account of their hydrophobic parts such as hydrocarbon chain, and methyl group (Brandstetter et al., 1996; Decker et al., 2006; Lew et al., 2000; Takeda et al., 1989; Zhang & Laursen, 1998), and like Ser, Asp, and Glu, these residues also provided contributions to hydrophobic interactions that may be as the result of constituting in a hydrophobic pocket/motif of their atoms (Biondi et al., 2000; Miyazawa et al., 2003; Mora et al., 2004). The key amino acid residues that the most

flavonoids and verapamil (positive control) interacted with were Arg258, Thr259, Phe263, Ser1113, Glu1115, Pro1116, Ile1117, and Arg1184. Among all of these; Arg258, Thr259, Phe263, Glu1115, Ile1117, and Arg1184 were identified by pharmacophore modelling suggesting occupying the same binding site of these flavonoid and the important role of these residues in stable holding the flavonoids as well as positive control in the binding cavity at ATP binding site of NBD2 resulting in prevention of ATP binding to the site.

Bioflavonoids possess antioxidant properties due to their conjugated π -electron systems that correlate with their P-gp inhibitory activity as shown in our QSAR study. Furthermore, the docked complexes were used to generate the pharmacophore models that illustrated significant contributions of the π -electrons in molecular binding interactions between the ligands and both NBDs and interestingly, it was found that, involving π systems, Leu906 was a key residue within the NBD1 binding site that contributes the leucine-aromatic interactions (Manas et al., 2004) with the benzene rings of flavonoids like formononetin, chrysin, floretin, and epigallocatechingallate (including the positive control; atorvastatin). The second key residue; Thr902 that possesses a polar hydroxyl group was important to contribute the side-chain polar group- π interaction (Kim et al., 1998; Liu et al., 1993; Love et al., 1996) with the benzene rings of epigallocatechin and demethylnobiletin (including atorvastatin). The third key residue; Lys532 was also identified. It contributed cation- π interactions with the benzene rings of morin and nobiletin. The key residues within NBD 2 binding site including Arg258 that contributed cation- π interaction with the ring C of robinin. After MD simulation, Tyr1129 contributed π - π interaction with the ring D of amorphigenin in the stable stage identified by the NBD2-amorphigenin pharmacophore modelling. Residue-based energy decomposition confirmed the contribution of Tyr1129 in the binding with π - π interaction between amorphigenin and NBD2 including Arg1184 that the residue generated cation- π interaction with ATP and may also contribute the same interaction with amorphigenin throughout the MD simulation. From the energy decomposition of chrysin, the result showed that Arg1229 may contribute the binding with a benzene ring of the ligand. The energy decomposition result of epigallocatechin emphasised that Arg258 is the hotspot residue of the ATP binding site within NBD2. This residue may contribute the cation- π interaction with benzene rings of

epigallocatechin as same as the initial binding interaction with the ring C of robinin. Moreover, the result pointed out that Tyr1040 and Phe 1082 of the binding site may be the key residues that contributed the π - π interactions with epigallocatechin. Regarding formononetin, the energy decomposition result showed the important role of Arg1218 in protein-ligand binding. This key residue may produce the cation- π interaction between formononetin and NBD2 throughout MD simulation which contributes the stable binding of the ligand within NBD2. As same as amorphenin, Arg1184 may be also a key residue that contributes in the cation- π interaction between NBD2 and rotenone, and including verapamil throughout the 15 ns simulations confirming the competitive mechanism of inhibition of flavonoids to prevent the ATP binding with its active site within NBD2. Other hotspot amino acid residues like Arg258 may contribute the cation- π interaction with verapamil all over the simulation as same as the initial interaction between this residue and robinin, and the dynamic molecular interaction between the residue and epigallocatechin, and moreover, Phe263 may favour the π - π interaction with this ligand. Our results suggest that π -electron plays a key role in the binding of flavonoids (including the controls containing aromatic rings within their molecules) with the ATP active sites within NBDs and physiochemical properties involving π -electrons of flavonoids correlated with a P-gp inhibitory activity via the ATP competitive mechanisms at NBDs.

Amorphigenin and formononetin are widely found in several species of Fabaceae (legume family) (Wink et al., 2012). Amorphigenin is present in *Amorpha fruticosa* isolated from the seedlings, seeds, and leaves and exhibited to have significant anti-proliferative activity, anti-cancer activity in many cell types, hepatoprotective activity and neuraminidase inhibition activity (Liang et al., 2015). Formononetin is isolated from *Astragalus membranaceus*. Its root of is a largely utilised Chinese medicinal plant that is famous for its vital-energy tonifying, skin reinforcing, tissue generative, abscess draining, diuretic, and actions. Formononetin is also found in the root of *Glycyrrhiza glabra* or *G. uralensis* (licorice), which have been largely utilised in China, Japan and the Western countries. The licorice extracts have generally been recognised as safe and are also used as flavouring and sweetening agents for chewing gums, candies, toothpaste, and beverages. Furthermore, formononetin is a main isoflavone ingredient of *Radix Astragali*. It is traditionally used for the treatment of diabetes, wound healing and

strengthening the immune system (Auyeung & Ko, 2010; Cho & Leung, 2007; Dong et al., 2007; Hoo et al., 2010). Chrysin was accounted to possess extensive spectrum biological activities. It was picked as marker for standardisation such as to ensure a consistent and acceptable quality some herbal products including *Oroxylum indicum*. *O. indicum* have been utilised as a single remedy or constitutive of famous Ayurvedic formulations. The root bark and stem bark of this plant have anti-allergic properties and are utilised in treatments of urticaria, asthma, allergic disorders, jaundice, sore throat, hoarseness, laryngitis, gastralgia, diarrhoea, dysentery, erythema and measles. This herb contains flavonoids including chrysin as active compound. Chrysin contents in *O. indicum* from root, stem, and leaf are 0.014, 0.004, and 0.007 percent respectively (Srinivas & Aparna, 2012). Moreover, chrysin is also found in propolis that has been utilised largely in traditional medicines for many years on account of the complex chemical constituents, and there is an attestation to instruct that propolis has various pharmaceutical properties along with antibacterial, antiviral, antitumor, anticancer, anti-inflammatory, and immunomodulatory. The presence of some flavonoids including chrysin can be utilised as a marker to differentiate propolis from other bee products. The content of chrysin has been utilised as a parameter for propolis quality. The amount of chrysin is nearly 15% (Zhou et al., 2008). *Scutellaria baicalensis* is one of the most largely utilised folk herbal remedies. Its roots have been utilised for anti-inflammation, anticancer, curing bacterial and viral infections of the respiratory and gastrointestinal tracts, clearing away heat, purging fire, moistening dryness, detoxifying toxicity, lowering blood pressure and total cholesterol level. Chrysin is likewise identified in underground and aerial parts of this plant (Li et al., 2004). Epigallocatechin is one of major catechins of green tea, brewed from the dried leaves of *Camellia sinensis* which is one of the most largely consumed beverages in the world (Velayutham et al., 2008). This compound possesses a high antioxidant activity (Almajano et al., 2008). Rotenone is commonly found in *Derris elliptica*, *D. scandens* and *Pachyrhizus erosus* (Fabaceae) (Bullangpoti, 2009). *D. scandens* is a medicinal plant ordinarily known in Thai as Thao-Wan-Priang. Its dried stem is utilised in Thai folk medicine as an antidysentery, expectorant, antitussive, diuretic, and treatment for muscle ache. It is verified that *D. scandens* can be utilised for health promotion in postmenopausal women, patients with cardiovascular diseases, and cancer prevention (Kuptniratsaikul et al., 2011).

P. erosus [English name: yam bean, Thai name: Man Kaeo, Huapaekua, Man Lao (Lim, 2016)], a horticultural crop, is used as food and cosmetic materials (Damayanti et al., 2008).

This study combines the molecular docking and MD simulation of P-gp inhibitors bound to NBD2. In previous studies illustrated that NBD2 could be the binding site for flavonoids. Realisation the mechanisms of how the inhibitor interacts with NBD is essential for screening of herb-drug interaction and the development of inhibitors that may overpower multidrug-resistant in human cells. The information of circumstantial atomic interactions between NBD2 and each flavonoid was obtained utilising pharmacophore modelling and MD simulation.

It has been suggested previously that hydrogen bonding interactions and hydrophobic interactions play important roles in the binding of flavonoids (Gadhe et al., 2013). This study supports that these interactions between NBD2–flavonoid could be of significant importance for the inhibition mechanism. All flavonoids (amorphigenin, chrysin, epigallocatechin, formononetin and rotenone) bind to ATP bind cavity of NBD2 and the binding was found to be stable throughout MD simulation. Backbone RMSD of NBD2 and ligands pointed out that they are steady after equilibration period. They bound with high negative binding energy values as same as the positive control and shows high potency towards P-gp inhibition. The hydrophobic interactions and hydrogen bonds were responsible for stable complex formation as revealed by the pharmacophore analysis and decomposed energies. Since each binding pose has not altered much during MD simulations, suggesting a vigorous binding between NBD2 and flavonoid. The results could be utilised henceforward for other flavonoid inhibitors which target NBD site. Finally, on the basis of data obtained during the study, it can be concluded that these bioflavonoids have the potential to cause herb-drug interactions or be used as lead molecules for the inhibition of P-gp (as anti-multidrug resistance agents) via the NBD2 blocking mechanism in future. This approach can be utilised to screen out a huge number of flavonoids for their potencies in anti-cancer treatments as well as herb-drug interactions.